

The Pennsylvania State University

The Graduate School

John and Willie Leone Family Department of Energy and Mineral Engineering

**WIND TUNNEL STUDY AND NUMERICAL ANALYSIS ON PARTICULATE MATTER
DISPERSION IN A THREE-DIMENSIONAL STREET CANYON**

A thesis in

Energy and Mineral Engineering

by

Mengfan Li

©2018 Mengfan Li

Submitted in Partial Fulfillment

of the Requirements

for the Degree of

Master of Science

December 2018

The thesis of Mengfan Li was reviewed and approved* by the following:

Jeremy M. Gernand

Assistant Professor of Industrial Health and Safety

Thesis Advisor

Mark S. Klima

Associate Professor of Mineral Processing and Geo-Environmental Engineering

Shimin Liu

Assistant Professor of Energy and Mineral Engineering

Luis F. Ayala H.

Professor of Petroleum and Natural Gas Engineering

Associate Department Head for Graduate Education

*Signatures are on file in the Graduate School

Abstract

This study aims to identify lower risk exterior shelter areas and building air intake locations by modelling particulate matter (PM) dispersion in a three-dimensional street canyon from a point source and comprises a wind tunnel experiment and a computational fluid dynamics (CFD) simulation. The model street canyon for this investigation was a two-by-two building matrix of constant height with aspect ratios of 0.35, 0.70, and 1.05. A PM emission source external to the street canyon simulated a scenario of an accidental point release. The experimental PM source was simulated with water droplets from an ultrasonic humidifier in the wind tunnel. The wind tunnel experiment provided the data to calibrate the CFD simulation, from which a wider set of results could be evaluated.

In the no-building case, measured PM concentrations from the wind tunnel experiment agreed with a modified Gaussian plume model of a continuous point source with a first-order decay term (adjusted $R^2 = 0.786$). The effective emission rate of the humidifier was estimated to be 5.27×10^6 particles/s. With street canyons, the association between a lower PM concentration and a greater aspect ratio contradicted past literature, mainly because the measurements locations were at the center of the internal intersection and the vertical vortices that could reduce street canyon ventilation capacity were absent in this experiment.

The CFD simulation produced PM concentrations with a relative deviation of 54.9% on average from those of the wind tunnel experiment. Inside the street canyon, the leeward sidewalks of the transverse exits had the lowest PM concentration at the breathing level of 1.5 m above the ground. Regardless of wind direction, PM source location, and aspect ratio, the top 1 m of and the bottom 1 m of any façade surface and the roof had the lowest PM concentration among all building surfaces with access to the internal intersection.

Therefore, if an accidental release of PM occurs and the source is identified as a point source outside the street canyons, pedestrians should move to the leeward sidewalks of the transverse exits, as other locations can have pedestrians exposed to at least a 60% higher PM concentration than the recommended evacuation site. For building construction and renovation, new ventilation air intakes should be installed at the top 1 m and the bottom 1 m of any façade surface and the roofs, as they registered up to 60.8% PM concentration at the unrecommended location in this scenario.

Table of Content

List of Figures	viii
List of Tables	xi
Acknowledgement	xii
1. Introduction.....	1
2. Literature Review.....	3
2.1. Street Canyons	3
2.2. Particulate Matter Dispersion in Street Canyons: Wind Tunnel Experiments.....	4
2.3. Particulate Matter Dispersion in Street Canyons: Computational Fluid Dynamics Simulations..	6
2.4. Motivation.....	7
2.5. Objectives	8
3. Methodology	9
3.1. Wind Tunnel Experiment.....	9
3.1.1. Location	9
3.1.2. Equipment	9
3.1.3. Wind Profiles	12
3.1.4. Model Similarity	13
3.1.4.1. Reynolds Number and Reynolds Number Independence	13
3.1.4.2. Rossby Number.....	13
3.1.4.3. Péclet Number.....	14
3.1.4.4. Froude Number	14
3.1.4.5. Boundary Conditions	14
3.1.5. Experimental Procedure.....	15
3.1.6. Modified Gaussian Plume Model.....	17
3.1.7. Other PM Transport Cases.....	19
3.2. CFD Simulation	20
3.2.1. Fluid Domain	21

3.2.2.	Mesh.....	22
3.2.3.	Boundary Conditions	23
3.2.4.	Numerical Models.....	23
3.2.4.1.	Turbulence Model: Standard $k - \epsilon$ Model	23
3.2.4.2.	Multiphase Model: Discrete Phase Model (DPM).....	25
3.2.5.	Model Calibration	26
4.	Results.....	28
4.1.	PM Dispersion without Street Canyon.....	28
4.1.1.	Wind Profiles	28
4.1.2.	Concentrations	29
4.1.3.	Dispersion Coefficients.....	30
4.1.4.	Modified Gaussian Plume Model.....	32
4.1.5.	Fate of PM.....	33
4.2.	PM Dispersion with Street Canyon.....	35
4.2.1.	Wind Profiles	35
4.2.2.	Concentrations	36
4.3.	CFD Simulation	36
4.3.1.	Model Calibration: Wind Profiles.....	36
4.3.2.	Model Calibration: Concentrations	39
4.3.3.	PM Concentrations at Breathing Height	40
4.3.4.	PM Concentrations along Building Façades	44
5.	Discussion.....	53
5.1.	Similarity between Wind Tunnel Experiment and CFD Simulation.....	53
5.2.	Prediction of PM Concentration with Decay Only	54
5.3.	Evacuation during Release Emergency.....	54
5.4.	Ventilation Air Intakes during Release Emergency.....	58
5.5.	Limitations	61

5.6. Future Work.....	63
6. Conclusion	64
References.....	66

List of Figures

Figure 2.1-1 Graphic illustration of street canyons with different aspect ratios from 0.5 to 3.0.	3
Figure 3.1-1 Graphic illustration of Irwin-type vortex generating spire.....	10
Figure 3.1-2 Wind tunnel setup of the first part: 50-cm downwind distance and 3-cm vertical distance...	16
Figure 3.1-3 Wind tunnel setup of the second part.	17
Figure 3.2-1 Graphic illustration of the fluid domain.	21
Figure 3.2-2 Graphic illustration of the mesh with wind coming from left.	22
Figure 3.2-3 Size distribution of water droplets in particle counts from an ultrasonic humidifier with a 0.44-m-long vinyl tube attached ⁴²	26
Figure 3.2-4 Locations of inlet profile, approach profile, and incident profile relative to buildings.....	27
Figure 4.1-1 Wind profiles for different fan operating frequencies. The frequencies of 8 Hz, 10 Hz, and 14 Hz had free stream wind velocities of 1.4 m/s, 1.6 m/s, and 2.2 m/s at 55.9 cm above the ground surface.	28
Figure 4.1-2 PM concentrations at 3 cm above the ground surface without street canyon.....	29
Figure 4.1-3 PM concentrations at 9 cm above the ground surface without street canyon.....	30
Figure 4.1-4 PM concentrations comparison between the modified Gaussian plume model and wind tunnel experiment data at 3 cm above the ground.....	32
Figure 4.1-5 PM concentrations comparison between the modified Gaussian plume model and wind tunnel experiment data at 9 cm above the ground.....	33
Figure 4.1-6 Predicted PM concentration at the centerline ground with PM transport cases of “no dispersion or decay”, “decay only”, “dispersion only”, and “dispersion and decay”.	34
Figure 4.1-7 Relative PM concentration change out of the total PM concentration change due to dispersion only and decay only. The total PM concentration change refers to the concentration differential between “no dispersion or decay” and “dispersion and decay”.	34
Figure 4.2-1 Wind profiles for different free stream velocities and different aspect ratios.	35

Figure 4.2-2 PM concentrations of open field and street canyons of different aspect ratios.	36
Figure 4.3-1 Wind profiles comparison among inlet profile, approach profile, incident profile, and experimental wind profiles.	37
Figure 4.3-2 Absolute wind velocity deviations of inlet profile, approach profile, and incident profile from experimental wind profiles.	38
Figure 4.3-3 PM Concentration comparison between CFD simulation and wind tunnel experiment data with street canyon.	39
Figure 4.3-4 Graphic illustration of names for different parts of a generic three-dimensional street canyon.	40
Figure 4.3-5 PM concentration contour and wind velocity vectors at the breathing height from CFD simulation with wind coming from the left. “Orange” indicates concentration higher than the 90 th percentile concentration, 2.11×10^7 particles/m ³ . “Red” indicates concentration higher than the 95 th percentile concentration, 3.73×10^7 particles/m ³	41
Figure 4.3-6 Mean PM concentrations in the transverse channel, the longitudinal entrance, and the longitudinal exit at the breathing height	42
Figure 4.3-7 Mean PM concentration at the leeward sidewalk, the windward sidewalk, and the transverse road at the breathing height.	43
Figure 4.3-8 Mean PM concentration within the leeward sidewalk. A crosswind distance of 0 m is at the longitudinal centerline, and a crosswind distance of 30 m is at the transverse exit.	44
Figure 4.3-9 PM concentration contour at the leeward façade surfaces of the transverse channel with wind coming out of the page. The longitudinal channel is to the left of the individual image.	46
Figure 4.3-10 PM concentration contour at the windward façade surfaces of the transverse channel with wind coming into the page. The longitudinal channel is to the left of the individual image.	47
Figure 4.3-11 PM concentration contour at the façade surfaces of the longitudinal entrance with wind coming from left. The transverse channel is to the right of the individual image.	48

Figure 4.3-12 PM concentration contour at the façade surfaces of the longitudinal exit with wind coming from the left. The transverse channel is to the left of the individual image.	49
Figure 4.3-13 PM Concentration contour at the roofs with wind coming from the left.	50
Figure 4.3-14 PM concentration highlighted map of any vertical façade surface regardless of wind velocity and wind direction. Locations with concentration below $1.54 \cdot 10^6$ particles/m ³ (the 50 th percentile concentration) are labeled green and those with concentration above $1.08 \cdot 10^7$ particles/m ³ (the 95 th percentile concentration) are labeled orange.	51
Figure 4.3-15 PM Concentration highlighted map of the roof regardless of wind velocity and wind direction. Locations with concentration below $1.54 \cdot 10^6$ particles/m ³ (the 50 th percentile concentration) are labeled green and those with concentration above $1.08 \cdot 10^7$ particles/m ³ (the 95 th percentile concentration) are labeled orange.	51
Figure 4.3-16 Ratio of mean PM concentrations at the top 1 m and bottom 1 m of any vertical façade surface and the roof to those at the remaining façade surface.	52
Figure 5.3-1 Ratio of PM concentrations at the longitudinal entrance and the longitudinal exit to those at the transverse channel at the breathing height.	55
Figure 5.3-2 Ratio of PM concentrations at windward sidewalks and transverse road to those at leeward sidewalks at the breathing level (1.5 m above the ground).	57
Figure 5.3-3 Recommended exterior shelter areas (green) for pedestrians during an accidental release from a site on the left.	58
Figure 5.4-1 Ratio of area less than the 50 th percentile concentration in the leeward façades to that in the windward façades.	59
Figure 5.4-2 Ratio of area with less than the 50 th percentile concentration in the longitudinal entrance to that in the longitudinal exit.	60
Figure 5.4-3 Recommended area (green) and compromised area (orange) for ventilation air intakes installation in a generic three-dimensional street canyon.	61

List of Tables

Table 3.2-1 Summary of empirical constants in the standard $k - \epsilon$ turbulence model³⁸ 24

Table 4.1-1 Summary of power law exponents for different free stream wind velocities. 28

Table 4.1-2 σ_y and σ_z estimations for each free stream velocity and downwind distance. Both tend to increase with a greater downwind distance..... 31

Table 4.1-3 Power coefficients estimations for σ_y and σ_z 31

Table 4.3-1 Summary of 50 percentile, 75 percentile, 90 percentile, 95 percentile, and 99 percentile concentrations at the breathing level (1.5 m above ground) from the CFD simulation. 40

Table 4.3-2 Summary of 50 percentile, 75 percentile, 90 percentile, 95 percentile, and 99 percentile concentrations at building façade surfaces from CFD simulation. 45

Acknowledgement

I would like first to express my gratitude to my advisor, Dr. Jeremy Gernand, of John and Willie Leone Family Department of Energy and Mineral Engineering. His generosity on his expertise in environmental risks and his passion in exploring air pollutant dispersion have been priceless treasure to me from the first day. Beyond the scope of academic project, his willingness of sharing his own thoughts on everyday topics also inspired me.

I would like also to express my gratitude to Dr. William Groves, Dr. Mark Klima, and Dr. Shimin Liu, of John and Willie Leone Family Department of Energy and Mineral Engineering. It was enormously kind of them to provide me the facility for the initial micro-scale wind tunnel experiment, essential equipment for the experiment, and the access to the underground wind tunnel at the Steidle Building.

I am also grateful to have my best friend, Shihwei Wang. Even though he was at Lehigh University at the time I devoted myself to the project, we were still constantly having academic discussion. The data analysis of the project benefitted tremendously from his statistical repertoire.

Finally, nothing can be achieved without a great family. My parents, Guangzhi Li and Huangying Chen, are extremely supportive of my choice to enroll in Integrated-Undergraduate-Graduate program at John and Willie Leone Family Department of Energy and Mineral Engineering and their expectation has always encouraged me.

Mengfan Li

1. Introduction

Air pollution has been discussed for millennia, but the types of air pollutants that caught attention have been constantly changing: after World War II, people were most concerned about sulfur dioxide (SO₂), whereas fast growing vehicle traffic increased the awareness of nitrogen oxides (NO_x) and volatile organic compounds (VOCs)¹. Not until the recent two decades did particulate matter (PM) become another prominent topic, as over a thousand papers focusing on PM are published annually, and PM represents two of the criteria air pollutants in the National Ambient Air Quality Standards (NAAQS)².

PM, also known as aerosols, is defined as a suspension of fine solids or liquid droplets in gas, whose aerodynamic diameter can range from a few nanometers (nm) to a few micrometers (μm)³. Emitted directly as particles (primary aerosols), or formed by gas-to-particle conversion processes (secondary aerosols), the majority of aerosols have anthropogenic origin, which contains sulfate, nitrate, black carbon, organics, and mineral dusts³. A common way to characterize PM is by its aerodynamic diameter. PM₁₀, PM_{2.5}, and ultrafine particles (PM_{0.1}) are the three categories that frequently appear in literature and regulations⁴. PM₁₀ and PM_{2.5} refer to the aerosols, whose aerodynamic diameter is less than 10 μm and 2.5 μm, respectively, and ultrafine particles refer to those with aerodynamic diameter less than 0.1 μm (or 100 nm).

PM is of concern due to its association with adverse health effects⁴. When humans are exposed to aerosols, most of them with aerodynamic diameter larger than 10 μm can be intercepted by the mouth or the nose, whereas up to 60% of PM₁₀ can pass the trachea and eventually deposit in the lung, so PM₁₀ and PM_{2.5} have been regulated by NAAQS since 1997⁴. While ultrafine particles are not currently monitored per NAAQS, they have been shown to be pathogenic in laboratory studies⁴.

PM concentrations in urban areas need continued attention. First, high outdoor PM concentrations can make exposed people susceptible to acute symptoms. On average, people spend 1.43 hours outdoors every weekday and 2.38 hours outdoors every weekend day⁵. However, even short exposure to high PM concentrations can lead to various acute respiratory effects, such as asthma attacks and decreased lung function⁶. Secondly, high outdoor PM concentrations can deteriorate indoor air quality through building air intakes⁷. Buildings are often installed with ventilation air intakes, but different locations of air intakes can be exposed to significantly varying PM concentration⁸.

Traffic emissions of PM have been frequently simulated with line sources in the urban area, as it accounts for up to roughly 40% of PM₁₀ on average⁴. However, point sources may better simulate the emissions from geological material, vegetative burning, industries, and accidental release emergencies, which are also identified as major contributor to PM concentrations⁴. This study simulates a scenario of PM being released from a point source outside a three-dimensional street canyon, and the results should help determine lower risk exterior shelter areas and building air intake installation locations.

2. Literature Review

2.1. Street Canyons

Street canyons are a product of urban development, as they are favorable for shelter and energy conservation with higher population density⁹. The name, street canyon, generally refers to semi-infinite two-dimensional cross-sections with intersections neglected; lower air quality is often associated with street canyons, compared to open areas, as local ventilation capacity is significantly reduced and vehicles can contribute additional pollutants. The phenomenon of street canyons leading to limited ventilation is known as the canyon effect¹⁰.

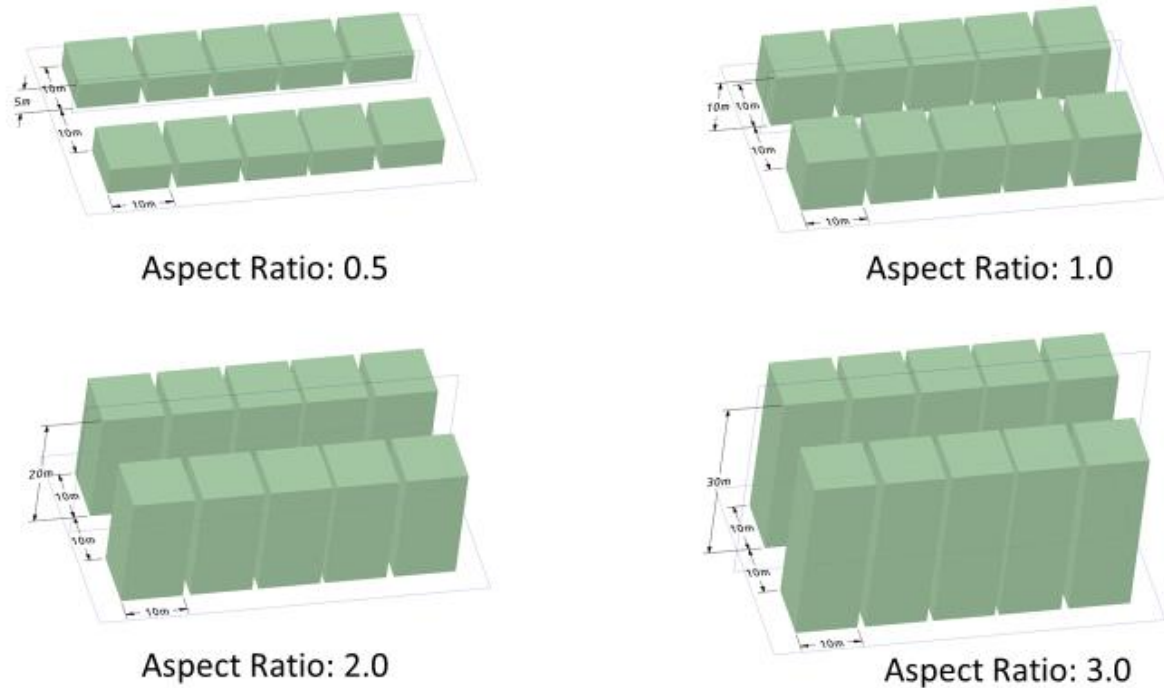


Figure 2.1-1 Graphic illustration of street canyons with different aspect ratios from 0.5 to 3.0.

Aspect ratio is one way to geometrically characterize street canyons and is defined as the ratio of the height of the buildings along the street to the width of the street. Street canyons with different aspect ratios can develop different flow patterns both inside and outside the canyon; as the aspect ratio increases,

the flow regime can be characterized into three categories, *isolated roughness flow regime*, *wake interference flow regime*, and *skimming flow regime*⁹. *Isolated roughness flow* occurs when the buildings are well apart with aspect ratio less than 0.3, as each flow field does not interact with each other. As the buildings become closer, forming a canyon with an aspect ratio between 0.3 and 0.75, *wake interference flow regime* is established, as the vortex at the windward side of the canyon is reinforced by downward wind deflected from the same side. When the aspect ratio is higher than 0.8, *skimming flow* occurs, characterized by a circulatory vortex being formed inside the canyon and the flow atop of the canyon not able to enter it⁹.

2.2. Particulate Matter Dispersion in Street Canyons: Wind Tunnel Experiments

Several preceding studies have explored how particulate matter (PM) dispersed in street canyons when street canyons were aligned perpendicularly to the wind direction. Emission sources were placed inside the street canyons and they were either continuous point sources or continuous line sources.

Higher concentrations were observed at the leeward side than those at the windward side, regardless of emission source configurations and street canyons geometries, which were building matrices or two rows of buildings^{8,11-14}. With an aspect ratio of 1.0, the leeward side could have up to ten times the concentration of the windward side at the lowest 10% of the street canyons height; when the aspect ratio was increased to 2.0, the leeward side could still triple the concentration of the windward side near the ground^{8,11}. Chang and Meroney suggested that the concentration deviation between the leeward side and the windward side dwindled when approaching the roof of street canyons, but the leeward side could still have up to four times more concentration than the windward side with an aspect ratio of 1.0⁸.

Various emission source configurations and different free stream wind velocities could also change concentrations at a particular location. Kastner-Klein and Plate suggested that a line source closer to the leeward side could double the concentration at the lowest 20% of the street canyon height at the leeward side, compared to a line source closer to the windward side, whereas the concentration deviation diminished when the sampling location was higher than 80% of the street canyon height¹¹. Rather, the concentration at the windward side was marginally affected with different line source locations¹¹. Free stream wind velocity is another factor in concentration at the leeward side and the windward side. Meroney et al. showed that concentrations inside street canyons decreased with increasing wind velocities ranging from 0.5 m/s to 5.0 m/s, but the rate of decrease became negligible when the wind velocity was greater than 3.0 m/s¹⁴.

Studies have disagreed on how aspect ratios affected concentrations at certain specific locations. Kastner-Klein and Plate had two parallel bars as street canyons in the reference case with two parallel line sources inside, and varied the aspect ratio from 0.5 to 2.0¹¹. They showed that the same sampling location recorded similar concentrations for different aspect ratios¹¹. Alternatively, Meroney et al. had a similar design, but it recorded higher concentration with higher aspect ratio, especially the leeward side, at which an increase from 0.5 to 1.0 in aspect ratio doubled the concentration¹⁴. Contradictory findings are likely to result from different free stream wind velocities. The study by Kastner-Klein and Plate showing minimal effect on concentration with different aspect ratios used a free stream wind velocity of 7.7 m/s, much higher than 2.0 m/s used by Meroney et al^{11,14}.

In addition to the leeward side and the windward side, the concentrations at the roof of street canyons were also influenced by variations in aspect ratio and free stream wind velocity. Meroney et al. showed that increasing pollutant concentrations could be found closer to the line source on the roof, and

concentrations were higher on the upwind side of the roof than the downwind side of the roof at equally distant sampling points¹⁴. Similar to the leeward side and the windward side, the roof had greater concentrations with a lower free stream wind velocity and a greater aspect ratio¹⁴.

2.3. Particulate Matter Dispersion in Street Canyons: Computational Fluid Dynamics Simulations

If physical models and computational fluid dynamics (CFD) models with similar building geometries and boundary conditions are compared, similar pollutant concentrations should be produced¹⁵⁻¹⁷. While the standard $k - \epsilon$ turbulence model was used with a two-dimensional street canyon containing a line source in the middle, the CFD simulation managed to produce a similar trend in pollutant concentrations, as the leeward side had a higher concentration than the windward side at all heights at an aspect ratio of 1.0^{15,17}. However, Chang and Meroney showed that when the street canyons became three-dimensional, the standard $k - \epsilon$ turbulence model overpredicted concentrations at the leeward and the windward sides, both by up to 200% higher, compared to its accompanied wind tunnel experimental data, but the concentration deviation reduced when closer to the roof⁸.

Aspect ratio and free stream wind velocity have been identified as main factors in simulated pollutant dispersion in street canyons^{15,17}. Chang and Meroney suggested that higher concentrations at the leeward and the windward sides near the ground were associated with a higher aspect ratio⁸. Huang et al. showed that a higher free stream wind velocity can lower overall concentration near the ground inside the street canyon¹⁷.

CFD models can also produce data that are often difficult or infeasible to obtain via wind tunnel experiments. Huang et al. suggested that the highest concentration at 15% of the street canyon height

occurred at 1/8 of the entire street width from the leeward wall, instead of right on the leeward wall, which could only register around 30% of the height concentration¹⁷.

2.4. Motivation

The studies mentioned in the preceding sections simplified the building geometries by merely including two-dimensional street canyons, except the one by Chang and Meroney^{8,11-17}. A three-dimensional street canyon can better resemble the building geometries commonly found in actual towns and cities. However, the work by Chang and Meroney cannot answer the question on how PM disperses in three-dimensional street canyons if the point source is placed outside the canyon, as not all PM originates within⁸. An accidental release outside the street canyon might as well bring PM concentrations above the established levels of concern inside street canyons. Predictions of where PM is most likely to be present at the highest concentrations is imperative to giving useful guidance to pedestrians in an evacuation and designing buildings to have the lowest risk internal environments.

Using gases can introduce inaccuracy in predicting PM dispersion, which was simulated by gaseous tracers, such as sulfur hexafluoride (SF₆), ethane (C₂H₆), krypton-85 (⁸⁵Kr), and carbon monoxide (CO)^{8,11-14}. The transport of gases is subject to thermodynamic diffusion, not a predominant transport mechanism for PM. Adopting a non-gaseous simulator of PM for wind tunnel experiments and CFD simulations can make such pollutant dispersion prediction relevant for some volatile organic compounds (VOC) with high molecular weights.

Moreover, the aforementioned studies focused on concentrations measured merely on the leeward and the windward sides, except the ones by Meroney et al. and Chang and Meroney, who also presented the concentration on the roofs of upwind and downwind buildings^{8,11-17}. However, pedestrians can still be

exposed to excessive amounts of PM at locations not included in the studies, such as in street canyon channel aligning along the wind direction. In addition to pedestrians, people inside buildings would also be vulnerable, had ventilation air intakes been installed at high concentration prone areas.

2.5. Objectives

This study aims to quantify expected PM concentrations along the streets and sidewalks at the breathing height and along building façade surfaces. These results can then provide short term evacuation and shelter guidelines for pedestrians on where to stay in an accidental release of PM and for the design of building ventilation air intakes regarding installation locations that are most likely to avoid the highest PM concentrations.

3. Methodology

The study consists of two main parts, the first being a wind tunnel experiment and the second being a computational fluid dynamics (CFD) simulation.

3.1. Wind Tunnel Experiment

A wind tunnel experiment was conducted at the Mining Ventilation Laboratory of the Steidle Building at The Pennsylvania State University. The experiment had two goals, first to provide particulate matter (PM) emissions concentration data for the calibration of the CFD simulation and second to estimate the descriptive parameters of PM emissions from an ultrasonic humidifier.

3.1.1. Location

The Mining Ventilation Laboratory is located underground in the Steidle Building, and the experiment was carried out in the outer loop of the laboratory, whose cross-section is 107 cm wide and 185 cm tall.

3.1.2. Equipment

The Mining Ventilation Laboratory is equipped with a digital drive, Yaskawa® P1000 Bypass, and a mining ventilation fan, SMJ HDA 42-17-1800 fan. The digital drive produced digital output from 8 Hz to 14 Hz during the experiment. The mining ventilation fan has an inner diameter of 106.7 cm. During the wind tunnel experiment, digital outputs of 8 Hz, 10 Hz, and 14 Hz produced free stream velocities of 1.4 m/s, 1.6 m/s, and 2.2 m/s, respectively. The free stream wind velocity is defined as the wind velocity not influenced by the spires and the Lego® blocks at the lowest elevation possible, and that lowest elevation is known as the height of the boundary layer.

Two folding tables were placed in series inside the wind tunnel. They served as the ground surface in the wind tunnel experiment. Each of them was 122 cm long, 60 cm wide, and 91 cm tall.

Four Irwin-type vortex generating spires were used to generate wind shear similar to atmospheric boundary flow, as shown in the study by Meroney et al.^{14,18}. Each spire consisted of a front face with a splitter plate attached in the back. The spires were 50 cm tall and 8 cm wide. During the experiment, they were placed 8 cm downwind from the front edge of the table and 8 cm crosswind from each other.

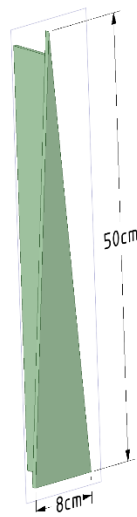


Figure 3.1-1 Graphic illustration of Irwin-type vortex generating spire.

Twelve Lego® blocks served as roughness elements to help achieve desired vertical wind profile^{12,14}. Each block was 1.5 cm long, 4.5 cm wide, and 0.95 cm tall. The blocks formed a four-by-three matrix, with gaps between rows and between columns both being 10 cm. The first row of blocks was placed 20 cm downwind from the spires.

Dry foam blocks from FLORACRAFT® were used to simulate urban buildings. Each dry foam block was 19.8 cm wide, 9.6 cm long, and 7.1 cm tall. Two pieces of dry foam together formed a single layer of building, with 19.8 cm in width, 19.2 cm in length, and 7.1 cm in height.

Shinyei PPD42NS dust sensors were used as PM sensors to detect water droplets in the experiment. They required a 5-volt direct current supply and created a digital signal called the Lo Pulse Occupancy Time when detecting particles with diameter larger than $1 \mu\text{m}$ ¹⁹. The signal could then be translated into particle counts in the unit of particles per cubic meter¹⁹. The opening of each PM sensor was 3 cm above its footing.

A DATAQ® DI-1100 data acquisition module was used to transfer sensor signals to a computer for recording and processing. The data acquisition module had a USB interface with 4 channels; each channel could have analog inputs from -10 volts to 10 volts, which covers the entire Shinyei PPD output range. The data file generated by DATAQ® DI-1100 is a type of WinDaq Waveform Browser HiRes Data File, with an extension name being WDH; it can be read by MATLAB®, once DATAQ® SDK .Net Class is installed on the computer²⁰.

HoldPeak® 866B digital vane anemometer was used to measure wind velocity. It had a vane diameter of 8.5 cm and could display wind velocity with precision of 0.1 m/s.

An ultrasonic humidifier from Homeleader® (model number: J04-017) was used to generate water droplets. It had a piezoelectric transducer located at the bottom of the humidifier, a transparent water storage tank, and a white cap with a discharge port of 1.27-cm diameter. The water storage tank could hold up to 1.6 L of water. During the operation, the humidifier was always set at maximum rate, and the

mean water consumption rate was estimated to be 112 ml/hr. Distilled water used in the ultrasonic humidifier was obtained from distilled water supply inside the Hosler Building at The Pennsylvania State University. Its hardness was less than 20 ppm.

A 50-cm-long polyvinyl chloride tube from EVERBILT™ was attached to the cap of the humidifier, so that the water droplets traveled through the tube before reaching the point of emission. Its inner diameter and outer diameter were 0.95 cm and 1.27 cm, respectively.

3.1.3. Wind Profiles

The wind profiles in the wind tunnel experiment were fitted with power law, an empirically developed relationship for wind shear²¹. It can be expressed as

$$\frac{u}{u_{ref}} = \left(\frac{z}{z_{ref}} \right)^\alpha \quad (1)$$

Where u is the wind velocity at the elevation of z , u_{ref} is the reference wind velocity at the reference elevation of z_{ref} , and α is the power law exponent²¹. In this wind tunnel experiment, u_{ref} used the free stream wind velocity and z_{ref} used the height of the boundary layer, which refers to the lowest elevation that wind velocity is free of influence from terrain and such velocity is free stream velocity. A greater value of α indicates a rougher terrain^{21,22}. McGowan has suggested that an α of $\frac{1}{7}$ is suitable for the investigators if they are simulating flat terrain, whereas the simulation of urban areas requires a higher value of α ²¹.

3.1.4. Model Similarity

A key concept that makes wind tunnel experimental results applicable to full-scale measurements is similarity²³. Generally, two turbulent flows are considered similar if and only if their Reynolds number (Re), Rossby number (Ro), Péclet number (Pe), Froude number (Fr), and boundary conditions are the same, and this principle can apply to both water and air²³. However, these criteria are almost impossible to meet simultaneously, so some less stringent metrics may be loosened without jeopardizing similarity²³.

3.1.4.1. Reynolds Number and Reynolds Number Independence

Reynolds number is defined as inertial force to viscous force. Had the criterion been strictly enforced that both model and prototype should have the same Reynolds number, no phenomenon in atmosphere could possibly be simulated in wind tunnels, because, for instance, a one-hundred-to-one reduction of length scale will result in a one-to-one-hundred increase of wind velocity²³.

Fortunately for wind tunnel experiments, a hypothesis known as *Reynolds number independence* enables wind tunnel models to replicate the prototypes in the atmosphere without having exactly the same Reynolds number; it states that “all geometrically similar flows are similar at all sufficiently high Reynolds numbers”²⁴. A Reynolds number can be considered “sufficiently high”, if it is greater than approximately 15000²⁵.

3.1.4.2. Rossby Number

Rossby number is defined as the ratio of local acceleration to Coriolis acceleration and is usually approaching infinity in wind tunnel experiments and therefore neglected²³. If the horizontal length scale is

less than tens of kilometers and the vertical length scale is less than one kilometer, Coriolis acceleration is minimal and the criterion can be ignored²⁶⁻²⁸.

3.1.4.3. Péclet Number

Péclet number is defined as the ratio of advective transport to diffusive transport and it is typically approaching infinity in wind tunnel experiments with flows at sufficiently high Reynolds number, and therefore neglected²³. It can also be viewed as the product of Reynolds number and Prandtl number. Prandtl number for air does not vary much with temperature, so Péclet number mainly depends upon Reynolds number.

3.1.4.4. Froude Number

Froude number is defined as the ratio of inertial force to buoyancy force and it can also approach infinity in wind tunnel experiments, when the atmosphere is of neutral stability there, and therefore neglected²³. The wind tunnel is too small in dimension to observe noticeable vertical temperature gradient, so the criterion of Froude number is relatively easy to meet.

3.1.4.5. Boundary Conditions

Other boundary conditions include fluid velocity, temperature, and pressure²³. If fans installed in wind tunnels have digital control, a specific free stream velocity can be easily met. If wind tunnels are connected to a room or placed inside a room, room temperature and atmospheric pressure can be therefore assumed.

3.1.5. Experimental Procedure

Four spires and twelve roughness elements were placed at the front part of the folding table. At 170 cm downwind from the spires, wind velocities at different heights were measured with the anemometer, after the mine ventilation fan was set to specific frequencies. During the experiment, frequencies of 8 Hz, 10 Hz, and 14 Hz were tested, the corresponding free stream velocities were 1.4 m/s, 1.6 m/s, and 2.2 m/s with corresponding Reynolds numbers of 54000, 62000, and 85000, respectively, all of which were greater than the threshold of Reynolds number independence of 15000²⁵.

The humidifier with a 50-cm long vinyl tube and three dust sensors were included for the first part of the experiment. The vinyl tube outlet was placed 120 cm downwind from the spires and at the longitudinal centerline of the ground surface. The ultrasonic humidifier was always operating at its maximum capacity, and the tube was fixed at the table pointing downwind. Three dust sensors were placed at the imaginary centerline, 5 cm and 7 cm crosswind from the centerline with their opening facing upwind. During the first part, PM concentrations were measured at three downwind distances from the tube outlet (40 cm, 50 cm, and 60 cm), two vertical distances from the table (3 cm and 9 cm), and three free stream velocities (1.4 m/s, 1.6 m/s, and 2.2 m/s). Measurements were repeated four times for the same downwind distance, vertical distance, and free stream velocity, and each lasted 5 min.

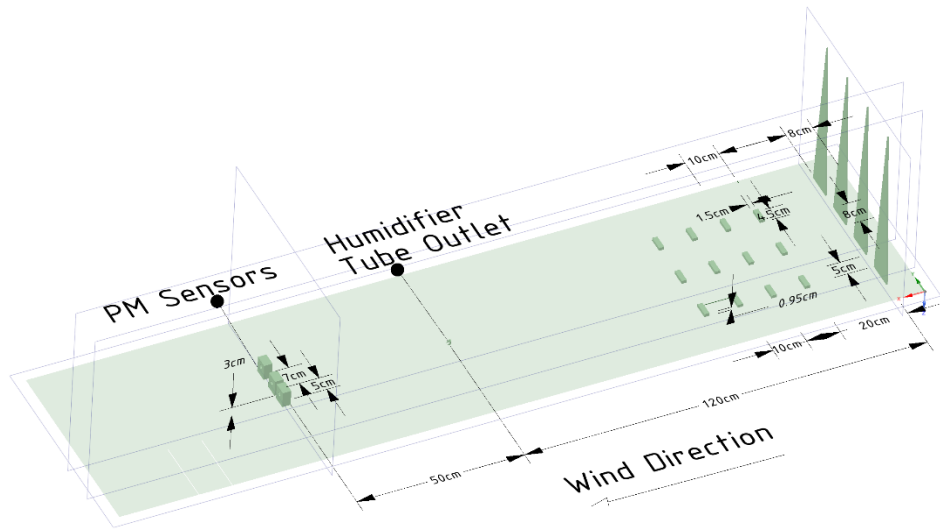


Figure 3.1-2 Wind tunnel setup of the first part: 50-cm downwind distance and 3-cm vertical distance.

Building models were added for the second part of the experiment. The front edge of the building was placed 20 cm downwind from the tube outlet. The dust sensors were always placed 50 cm downwind from the tube outlet, so that they were at the center of the street canyon. The distances between sensors were kept the same. PM concentrations were measured at 3 cm above the table with building configurations of single layer (aspect ratio of 0.35), double layer (aspect ratio of 0.70), and triple layer (aspect ratio of 1.05) and free stream velocities of 1.4 m/s, 1.6 m/s, and 2.2 m/s. Before concentration measurements, wind velocities at different heights were measured at the center of the street canyon, which was 50 cm downwind from the tube outlet. Similar to the first part, measurements were repeated four times for the same building configuration and free stream velocity, and each lasted 5 min.

and x , y , and z are three Cartesian coordinates. If σ_y and σ_z are considered functions of x , they will be fitted with Brookhaven National Laboratory formula in form of $\sigma = ax^b$, with x in unit of m^{29} .

Alternatively, σ_y and σ_z can be determined directly from the data obtained from the experiment. The calculation is based on the definition, that they are the standard deviations of concentrations in crosswind and vertical directions, respectively³⁰. From analogy to the normal distribution, σ_y and σ_z can be expressed as

$$c = \frac{1}{\sqrt{2\pi\sigma_y^2}} * \exp\left[-\frac{(y-\mu_y)^2}{2\sigma_y^2}\right] \quad (3)$$

$$c = \frac{1}{\sqrt{2\pi\sigma_z^2}} * \exp\left[-\frac{(z-\mu_z)^2}{2\sigma_z^2}\right] \quad (4)$$

Since the reference of crosswind distance is taken at the longitudinal centerline and that of vertical distance is taken at the ground, both μ_y and μ_z become 0.

Parameters from the modified Gaussian plume model were estimated in MATLAB®. An initial estimation was performed using random values for all four parameters, $Q_{effective}$, k , a_y , b_y , a_z , and b_z . A built-in function, *patternsearch*, was used to refine the initial estimation by looking for one that produces least absolute residuals between the concentration data and the modified Gaussian plume model. Another built-in function, *nlmfit*, was used to produce the parameters estimation.

Structurally, a computational loop was created, so that the parameters estimation in this iteration became the initial estimation in the next iteration. The loop would not stop until the relative errors between each

pair of parameters in the initial estimation and the parameter estimation was less than a pre-defined relative error threshold of 0.1%.

3.1.7. Other PM Transport Cases

Besides the modified Gaussian plume model, which characterizes the PM transport with both dispersion and decay, other PM transport cases are also considered, including the transport without dispersion or decay, the transport with dispersion only, and the transport with decay only. The differential between cases will be used to quantify the respective contribution of dispersion and decay to PM concentration change.

The turbulent diffusion of an inert pollutant can be characterized by

$$\frac{\partial \bar{c}}{\partial t} + \bar{u}_j \frac{\partial \bar{c}}{\partial x_j} = \frac{\partial}{\partial x_j} \left(K_j \frac{\partial \bar{c}}{\partial x_j} \right) \quad (5)$$

Where \bar{c} is the mean concentration of PM in Reynolds decomposition, \bar{u}_j is the mean wind velocity in Reynolds decomposition, and K_j is eddy diffusivity³⁰. If the x direction is built arbitrarily along the wind direction, the transport of the pollutant is deemed steady-state, and it only travels strictly downwind due to advection by wind, Equation (5) becomes

$$u \frac{d\bar{c}}{dx} = K_x \frac{d^2 \bar{c}}{dx^2} \quad (6)$$

If only downwind portion is considered, the particular solution to Equation (6) is given by

$$\bar{c} = \frac{Q_{effective}}{A * u} \quad (7)$$

Where A is the cross-section area of the source, which is the cross-section area of the vinyl tube³¹.

Equation (7) will be used as the model for PM transport case of *no dispersion or decay*.

If only decay needs to be considered here, the mean concentration of PM at the ground centerline is given by

$$\bar{c} = \frac{Q_{effective}}{A * u} * exp\left(-k * \frac{x}{u}\right) \quad (8)$$

Extra caution is required before the results are interpreted, because the decay coefficient, k , is estimated from the case that the decay coexists with the dispersion, and its value can be unreliable in the case that PM count density is far greater than the previous one. Equation (8) will be used as the model for the PM transport with *decay only*.

If only dispersion needs to be considered here, the mean concentration of PM at the ground centerline is given by the original Gaussian plume model,

$$\bar{c} = \frac{Q_{effective}}{2\pi u \sigma_y \sigma_z} \quad (9)$$

The values of σ_y and σ_z come from the fitted regression results of the modified Gaussian plume model in Equation (2). Equation (9) will be used as the model for the PM transport with *dispersion only*.

3.2. CFD Simulation

CFD simulation was carried out with the software, ANSYS® FLUENT. The objective of the simulation was to predict local maxima and minima of PM concentrations, simulated by water droplets, at 1.5 m above the ground and along building façade surfaces. The CFD model was calibrated with the data obtained in the wind tunnel experiment.

3.2.1. Fluid Domain

The fluid domain should be created large enough that no artificial acceleration would be induced and flow could be fully developed³². As suggested by Tominaga et al., Franke et al., and Franke and Baklanov, the inlet, top, and lateral boundaries should be at least $5H$ away from the buildings of interest, where H refers to the height of the tallest part of the building; furthermore, the outlet should be at least $15H$ behind the building^{33–35}.

The model in ANSYS® FLUENT had a scaling ratio of 100:1 compared to the street canyon in the wind tunnel experiment. The emission source, simulating the humidifier outlet, was on the ground and 20 m upwind from the front edge of the street canyon. Each block of building was 20 m in length and width and every layer was 7 m in height. The entire domain was 960 m long, 660 m wide, and 360 m tall. The inlet of the fluid domain was 300 m upwind from the front edge of the building matrix, lateral and top boundaries were 300 m from the closest lateral edges, and the outlet was 600 m downwind from the back edge.

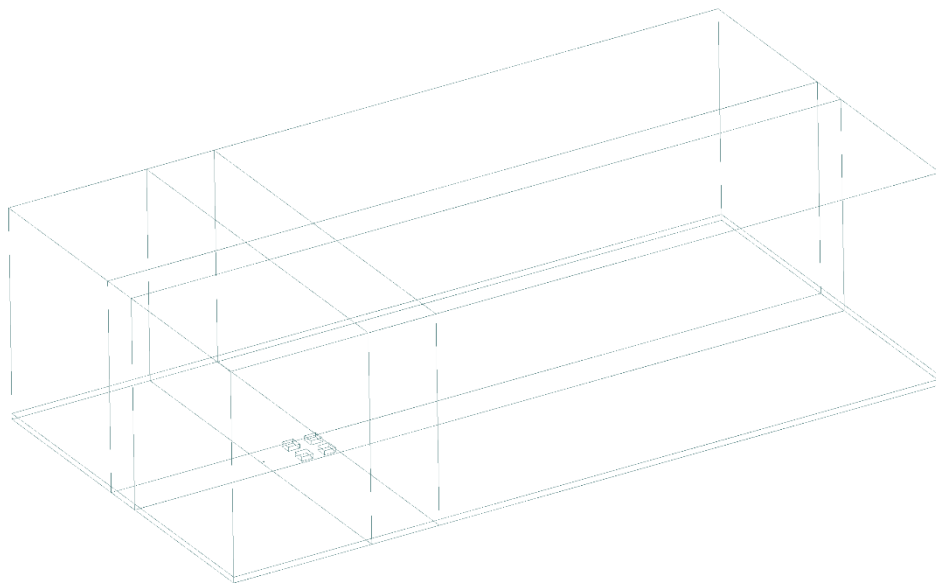


Figure 3.2-1 Graphic illustration of the fluid domain.

3.2.2. Mesh

A large fluid domain is divided into smaller computational grids to increase accuracy, and this process is called discretization. Computational grids should be set up small enough that the important physical phenomena could be captured, such as shear layers, and more grids should be present where critical variables might be observed with high gradients^{34,35}. Various shapes of computational grids are available in commercial CFD software, but Hirsch, Bouffieux, and Wilquem suggested that hexahedra be used rather than tetrahedra, because the former has smaller truncation errors and therefore has better convergence³⁶.

In this study, the entire fluid domain was discretized into tetrahedral cells. Meshing methods of sizing and refinement were used to create finer cells near the emission source and the buildings. The size of cells ranges from 1 m near building façades to 5 m at the wind-approaching region.

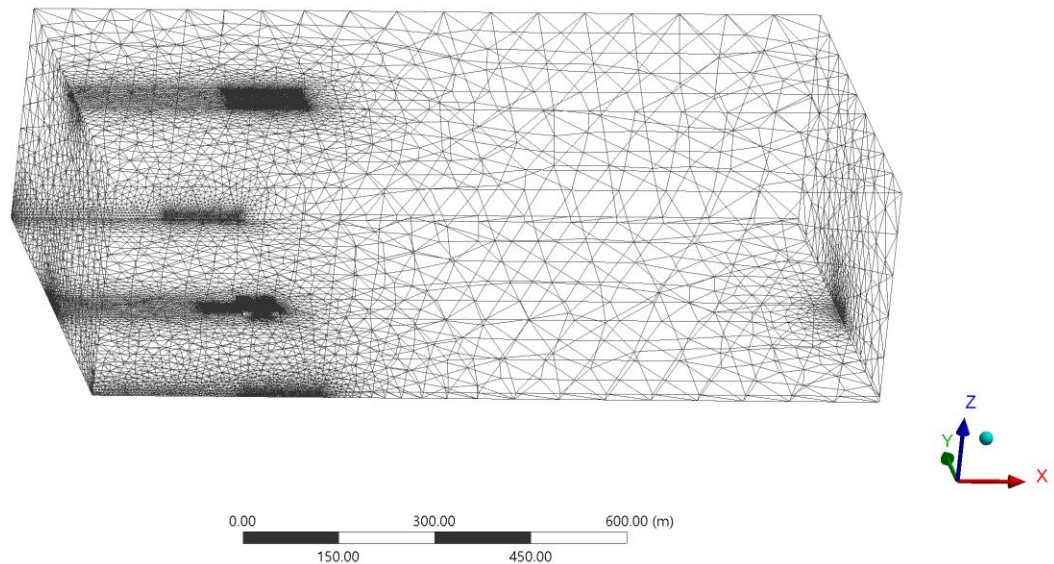


Figure 3.2-2 Graphic illustration of the mesh with wind coming from left.

3.2.3. Boundary Conditions

ANSYS® FLUENT allows users to choose from a number of prescribed boundary conditions to fulfill their needs³⁷. In this study, domain inlet was set to *velocity inlet*, a common boundary condition to introduce incompressible fluid flow into the domain with either uniform or customized vertical velocity profile; lateral and top boundaries were set to *symmetry*, at which zero normal velocity gradient and zero pressure gradient were present; domain outlet was set to *outflow*, at which the gradients of all variables became zero except pressure; the ground and the buildings were set to *no-slip wall*, at which the fluid velocity becomes zero^{32–35,37}.

The wind velocity profiles from the wind tunnel experiment were introduced normal to the domain inlet with heights scaled up according to the ratio for corresponding free stream wind velocities. Turbulence intensity and turbulence length scale were set at 15% and 1 m, respectively. A roughness length of 1.5 m was imposed on the ground, as it is a suitable value for urban environment²¹.

3.2.4. Numerical Models

In ANSYS® FLUENT, a turbulence model was used to simulate continuous phase in the domain and a multiphase model was used to simulate pollutant dispersion. To clarify, the term, “multiphase model”, refers to any model that introduces a phase other than the continuous phase, rather than the particular model in the software, “Multiphase Model”.

3.2.4.1. Turbulence Model: Standard $k - \epsilon$ Model

The standard $k - \epsilon$ turbulence model, a steady-state calculation under the category of Reynolds-average Navier-Stokes (RANS) approach, was used to simulate the movement of the continuous phase in the fluid

domain. Standard wall functions were set for near-wall treatment. Second order upwind spatial discretization for turbulent kinetic energy (k) and turbulent dissipation rate (ϵ) were used in the pressure-velocity coupled solver.

Two governing equations for the standard $k - \epsilon$ turbulence model are

$$\frac{\partial k}{\partial t} + \frac{\partial k u_j}{\partial x_j} = \frac{1}{\rho} \frac{\partial}{\partial x_j} \left(\frac{\mu_t}{\sigma_k} \frac{\partial k}{\partial x_j} \right) + \frac{\mu_t}{\rho} \left(\frac{\partial u_i}{\partial x_j} + \frac{\partial u_j}{\partial x_i} \right) \frac{\partial u_i}{\partial x_j} - \epsilon \quad (4)$$

$$\frac{\partial \epsilon}{\partial t} + \frac{\partial \epsilon u_j}{\partial x_j} = \frac{1}{\rho} \frac{\partial}{\partial x_j} \left(\frac{\mu_t}{\sigma_\epsilon} \frac{\partial \epsilon}{\partial x_j} \right) + \frac{C_1 \mu_t \epsilon}{\rho k} \left(\frac{\partial u_i}{\partial x_j} + \frac{\partial u_j}{\partial x_i} \right) \frac{\partial u_i}{\partial x_j} - C_2 \frac{\epsilon^2}{k} \quad (5)$$

Where k represents turbulent kinetic energy, ϵ represents the rate of dissipation of turbulent kinetic energy per unit mass, ρ represents the density of fluid, μ_t represents eddy diffusivity, and σ_k , σ_ϵ , C_1 , and C_2 are empirical constants³⁸. μ_t can be expressed as

$$\mu_t = C_\mu \rho \frac{k^2}{\epsilon} \quad (6)$$

Where C_μ is another empirical constant³⁸. The values for all five empirical constants were determined from experiments, and are shown at Table 3.2-1.

C_μ	C_1	C_2	σ_k	σ_ϵ
0.09	1.44	1.92	1.00	1.30

Table 3.2-1 Summary of empirical constants in the standard $k - \epsilon$ turbulence model³⁸.

Other commonly used turbulence models are Reynolds stress model (RSM) and detached eddy simulation (DES). Both are transient calculations and more suitable for urban environment, in which air pollutants transport is essentially unsteady, but their demand on computational resources can be too high^{8,39}.

Alternatively, the RANS approach is a steady-state calculation and has a balance between lower computational capacity demand and satisfactory calculation accuracy³⁹.

3.2.4.2. Multiphase Model: Discrete Phase Model (DPM)

In ANSYS® FLUENT, DPM allows users to simulate a discrete second phase in the Lagrangian frame⁴⁰. The fundamental assumption of DPM is that the discrete phase takes up low volume fraction, usually less than 10% to 12% of the entire fluid domain^{40,41}. In DPM, both steady-state and transient simulations can be implemented, different types of second phase flows can be chosen, and droplet collision and coalescence can be modelled if necessary.

Interaction with the continuous phase, unsteady particle tracking, and stochastic tracking with discrete random walk model were enabled. Particle tracking length scale was 0.5 m and the number of time steps was 3000 with particle time step size being 1 s. Runge-Kutta was used in high order scheme.

The particles introduced in DPM after 1000 iterations were named as ‘water-vapor’ and made as ‘inert’. A total duration of 1000 s was simulated. The emission rate was 0.0025 kg/s. The size distribution of water droplets by counts was documented in a previous study by Rodes et al., which used an ultrasonic humidifier with a 0.44-m-long vinyl tube attached and was described by Rosin-Rammler distribution⁴². Minimum diameter was 9.49×10^{-7} m, maximum diameter was 1.05×10^{-5} m, mean diameter was 2.928×10^{-6} m, and spread parameter was 1.7650. Additionally, 1 kg of water droplets contains 3.297×10^{13} particles on average, and the conversion is critical, as concentrations from dust sensors are expressed in particles/m³ but those in CFD are in kg/m³.

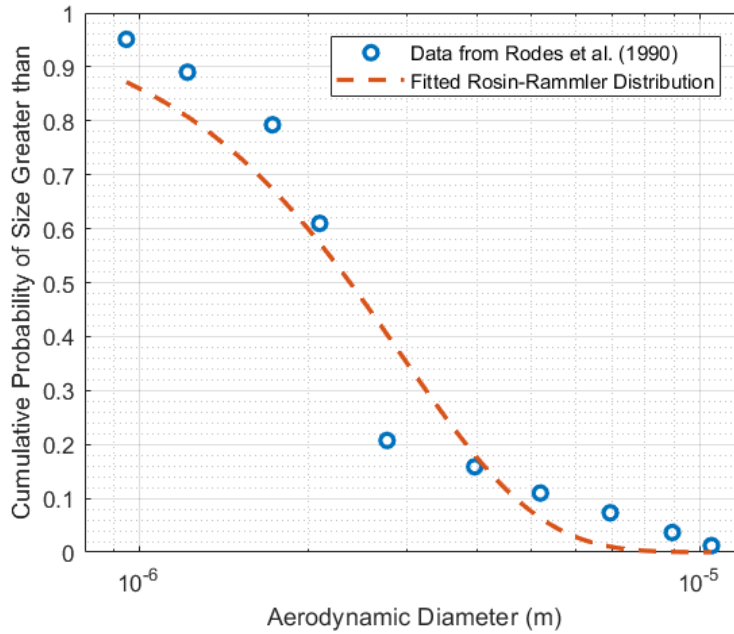


Figure 3.2-3 Size distribution of water droplets in particle counts from an ultrasonic humidifier with a 0.44-m-long vinyl tube attached⁴².

Regarding the mass concentration of second phase flows, it is governed by the equation

$$\frac{\partial}{\partial x_j} \left(\rho u_j C_i - \frac{\mu_t}{Sc_t} \frac{\partial C_i}{\partial x_j} \right) = S \quad (7)$$

Where C_i is mean air pollutant concentration, Sc_t is turbulent Schmidt number ($Sc_t = 0.9$), and S is air pollutant source term⁴³.

3.2.5. Model Calibration

Since two phases are modelled in the fluid domain, the model calibration can be done in two parts, one for the continuous phase and one for the discrete phase.

Regarding the continuous phase, air, models are calibrated by comparing different vertical wind profiles from the wind tunnel experiment and CFD simulation⁴⁴. The purpose is to ensure that the wind profiles are well maintained from the domain inlet to the building, as the wind profiles obtained from the wind tunnel experiment are introduced at the domain inlet. For each free stream velocity, there are three important wind profiles: inlet profile, approach profile, and incident profile⁴⁴. Inlet profile refers to the wind profile at the inlet of the fluid domain. Approach profile refers to the wind profile at the front vicinity of buildings. Incident profile refers to the wind profile, at which the buildings would be placed later.

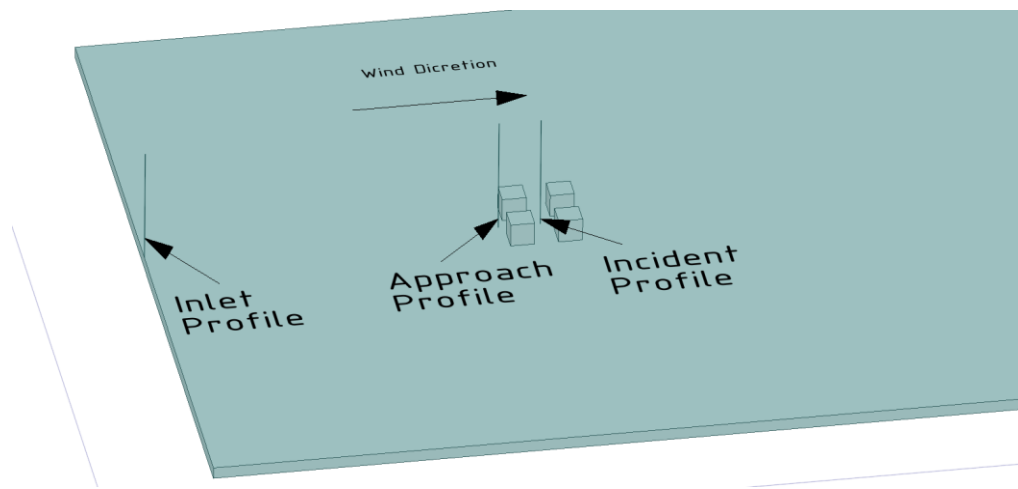


Figure 3.2-4 Locations of inlet profile, approach profile, and incident profile relative to buildings.

Regarding the discrete phase, models are calibrated by comparing pollutant concentrations from the wind tunnel experiment and CFD simulation^{8,15-17}.

4. Results

4.1. PM Dispersion without Street Canyon

4.1.1. Wind Profiles

Power law regression was used to fit the wind profiles of three free stream wind velocities. The reference elevation was 55.9 cm, and the reference wind velocities were their corresponding free stream wind velocities. The exponent, α , associated with the free stream wind velocity of 1.6 m/s is typically found in small towns and suburbs, whereas the other two can be found in urban areas with tall buildings²¹.

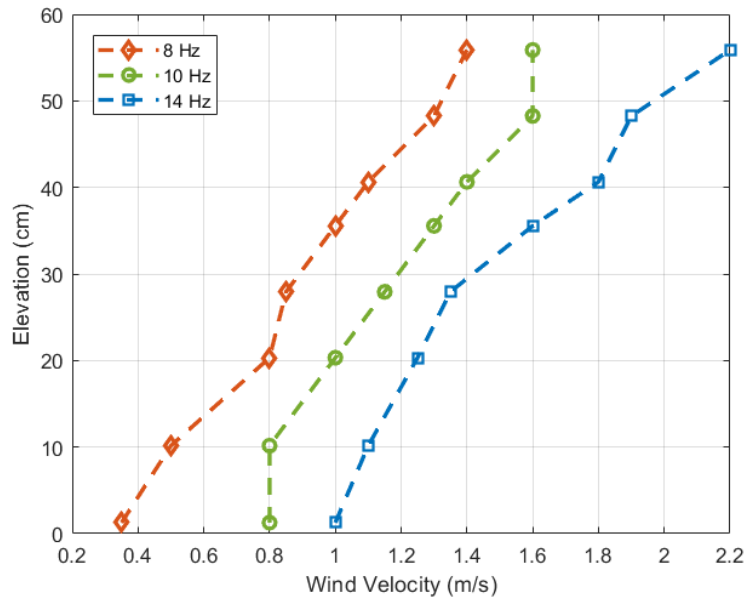


Figure 4.1-1 Wind profiles for different fan operating frequencies. The frequencies of 8 Hz, 10 Hz, and 14 Hz had free stream wind velocities of 1.4 m/s, 1.6 m/s, and 2.2 m/s at 55.9 cm above the ground surface.

Free Stream Wind Velocity (m/s)	1.4	1.6	2.2
α	0.5808	0.3167	0.4119
α 95% Confidence Interval	(0.4489, 0.7127)	(0.1890, 0.4443)	(0.2192, 0.6047)

Table 4.1-1 Summary of power law exponents for different free stream wind velocities.

4.1.2. Concentrations

When the PM sensors were placed 3 cm above the table, PM concentrations across crosswind distances resembled the bell shape of a normal distribution, and they decreased with greater downwind distances, as shown in Figure 4.1-2. As the free stream velocity increased, PM concentrations decreased, except for the PM sensor with the crosswind distance of 0 cm and the downwind distance of 40 cm. Different responses are expected, as not only can a higher free stream velocity increase the concentration by pushing more PM towards sensors with shorter distance, but also decrease the concentration by accelerating evaporation process with longer distance. When the PM sensors were placed 9 cm above the table, the bell shape was still well maintained, except for the data at the downwind distance of 60 cm, as shown in Figure 4.1-3. PM concentrations at the downwind distance of 50 cm were higher than those at 40 cm.

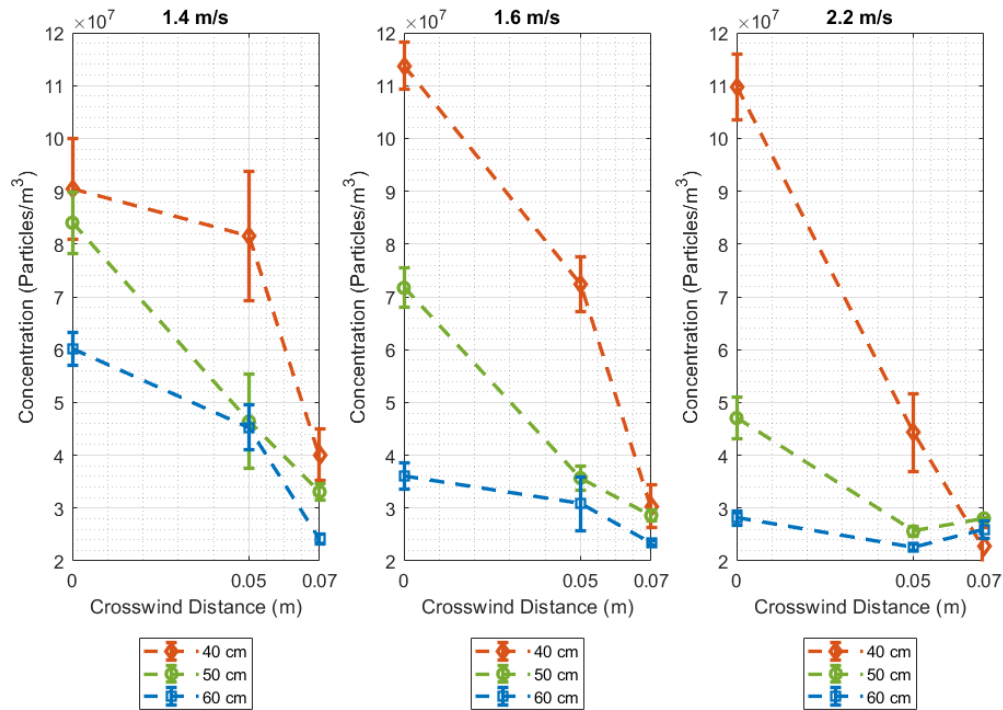


Figure 4.1-2 PM concentrations at 3 cm above the ground surface without street canyon.

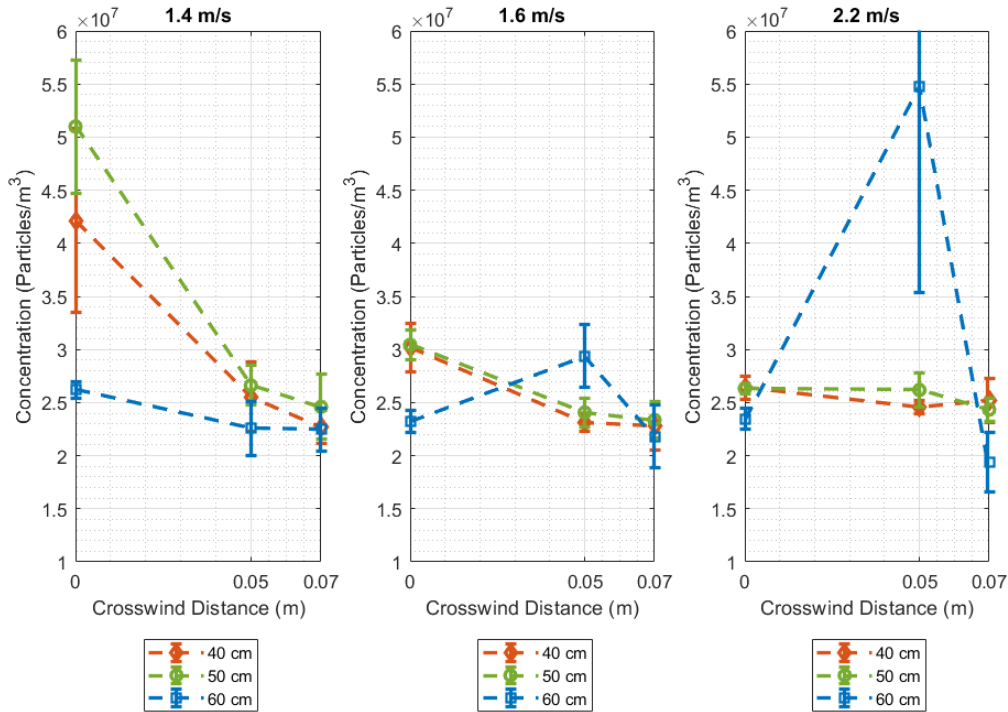


Figure 4.1-3 PM concentrations at 9 cm above the ground surface without street canyon.

4.1.3. Dispersion Coefficients

The calculations for both σ_y and σ_z in this section are based on the definition that they are the standard deviations of PM concentration in crosswind and vertical directions, respectively³⁰. σ_y and σ_z were estimated to be 6.66 cm and 8.84 cm, respectively. Both fall in the range of crosswind and vertical distances tested.

Individual estimations of σ_y and σ_z increased with greater downwind distance as expected. In the conventional Gaussian plume model, both σ_y and σ_z have similar characteristics, as plumes tend to disperse more laterally and vertically with longer travel time.

Free Stream Velocity (m/s)	Downwind Distance (cm)	σ_y (cm)	σ_z (cm)
1.4	40	5.93	6.20
	50	5.45	8.29
	60	8.83	6.88
1.6	40	6.80	5.41
	50	7.37	8.02
	60	13.26	19.31
2.2	40	12.96	6.46
	50	12.27	7.89
	60	14.19	14.12

Table 4.1-2 σ_y and σ_z estimations for each free stream velocity and downwind distance. Both tend to increase with a greater downwind distance.

Both σ_y and σ_z are fit with Brookhaven National Laboratory formula in form of $\sigma = ax^b$, with x in units of m^{29} . One-way analysis of variance (ANOVA) was run. Regarding σ_y , the coefficient b was not statistically different from 0 ($p = 0.2516$). Regarding σ_z , the coefficient b was statistically different from 0 ($p = 0.0203$).

	a	a Confidence Interval	b	b Confidence Interval
σ_y	0.242	(-1.399, 1.883)	0.943	(-0.775, 2.661)
σ_z	0.00181	(-0.0133, 0.0169)	2.171	(0.0894, 4.252)

Table 4.1-3 Power coefficients estimations for σ_y and σ_z .

4.1.4. Modified Gaussian Plume Model

Effective emission rate ($Q_{effective}$) and decay coefficient (k) were estimated to be 5.27×10^6 particles/s (standard error: 72 particles/s) and 1.41 s^{-1} (standard error: 0.10 s^{-1}), respectively. The fitted coefficients for horizontal dispersion coefficient (a_y and b_y) and vertical dispersion coefficient (a_z and b_z) within the modified Gaussian plume model were estimated to be 0.092 (standard error: 0.014), 0.65 (standard error: 0.18), 0.20 (standard error: 0.032), and 1.29 (standard error: 0.19), respectively. Adjusted coefficient of determination (Adjusted R^2) was 78.6%. The same set of experimental parameters (x, y, z, u) were used with the modified Gaussian plume model to predict the concentration, as shown in Figure 4.1-4 and Figure 4.1-5. At both z 's, the predicted concentrations were in the same order of magnitude with the experimental data. Good agreement could be found when z was 3 cm.

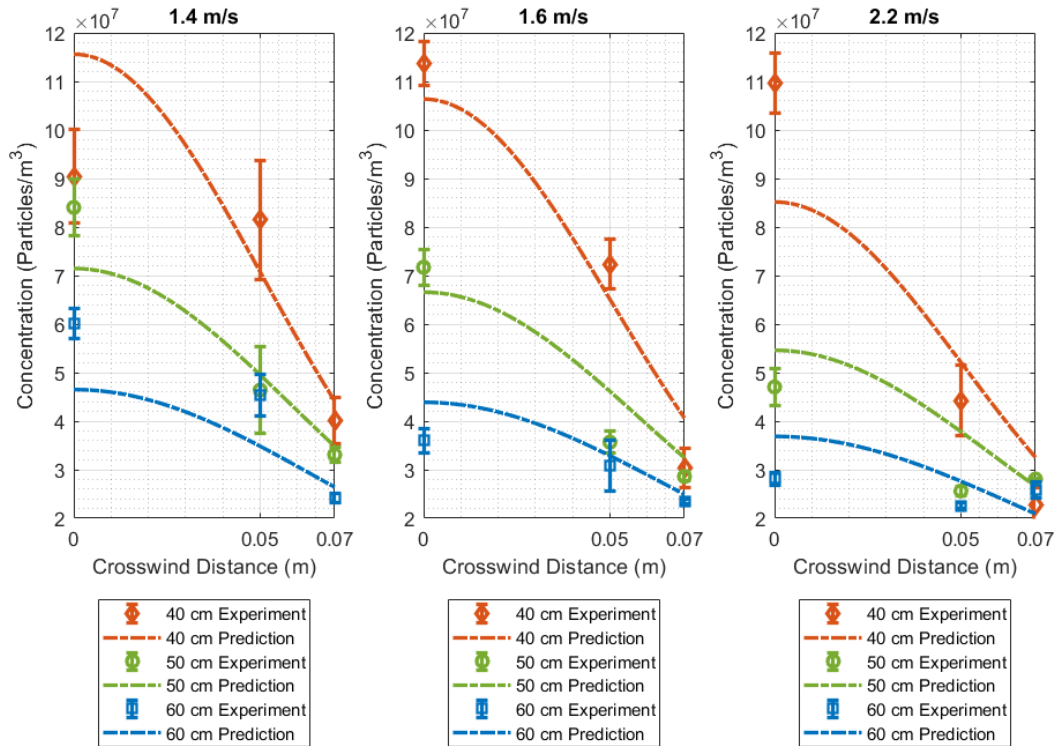


Figure 4.1-4 PM concentrations comparison between the modified Gaussian plume model and wind tunnel experiment data at 3 cm above the ground.

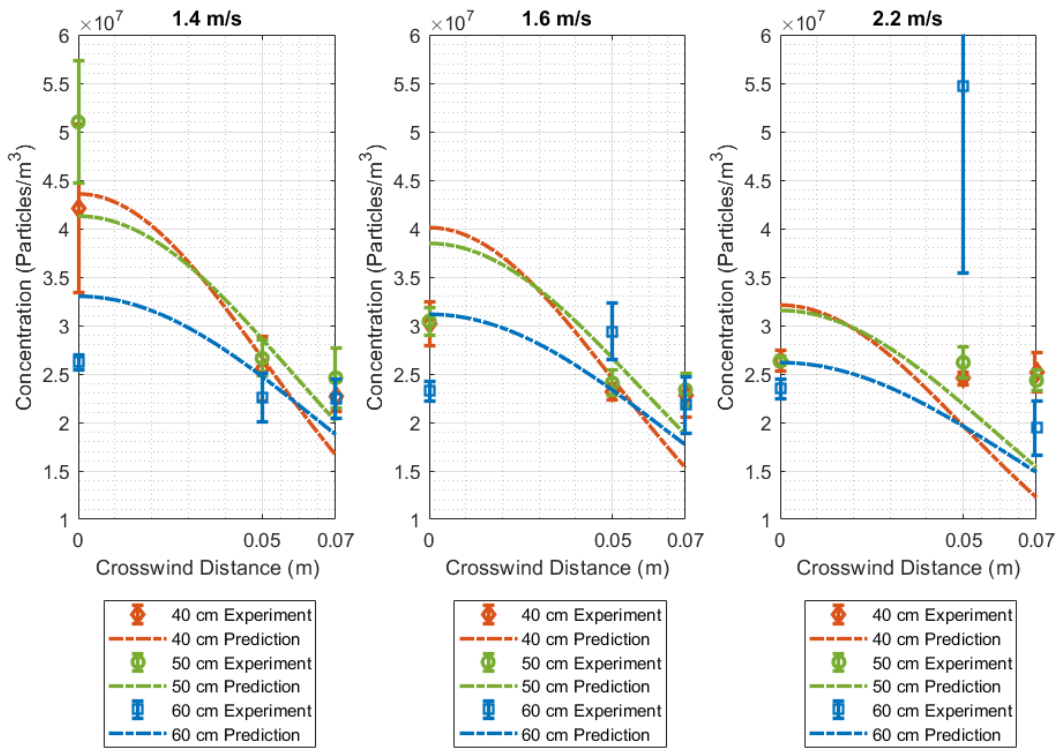


Figure 4.1-5 PM concentrations comparison between the modified Gaussian plume model and wind tunnel experiment data at 9 cm above the ground.

4.1.5. Fate of PM

In this experiment, PM was simulated by water droplets, whose dispersion and decay could contribute to concentration loss at the centerline ground. When both dispersion and decay were taken out of the PM transport, the PM concentration was constant with respect to downwind distance and could be as high as 5.3×10^{10} particles/m³ with free stream wind velocity of 1.4 m/s in Figure 4.1-6. The addition of decay alone decreased the PM concentration by less than 50%, but the addition of dispersion alone made the PM concentration drop substantially as shown in Figure 4.1-7.

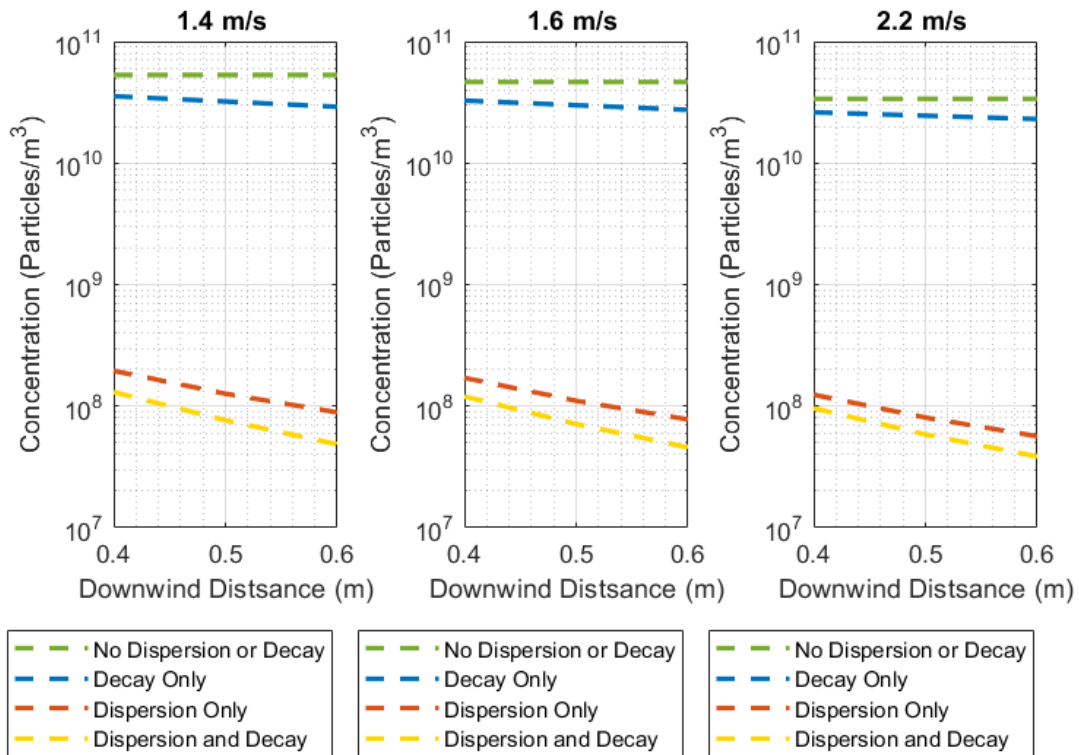


Figure 4.1-6 Predicted PM concentration at the centerline ground with PM transport cases of “no dispersion or decay”, “decay only”, “dispersion only”, and “dispersion and decay”.

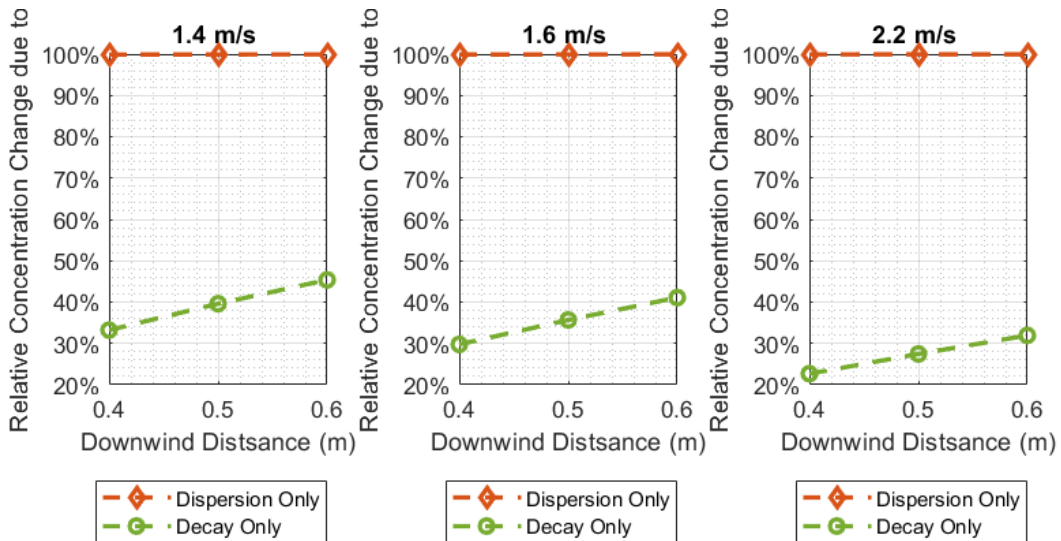


Figure 4.1-7 Relative PM concentration change out of the total PM concentration change due to dispersion only and decay only. The total PM concentration change refers to the concentration differential between “no dispersion or decay” and “dispersion and decay”.

4.2. PM Dispersion with Street Canyon

4.2.1. Wind Profiles

In general, wind profiles shifted to the right with a greater aspect ratio, and the most apparent right shift could be witnessed at the free stream wind velocity of 1.4 m/s, as shown in Figure 4.2-1. Wind profile variations among different aspect ratios were the least at the free stream wind velocity of 2.2 m/s.

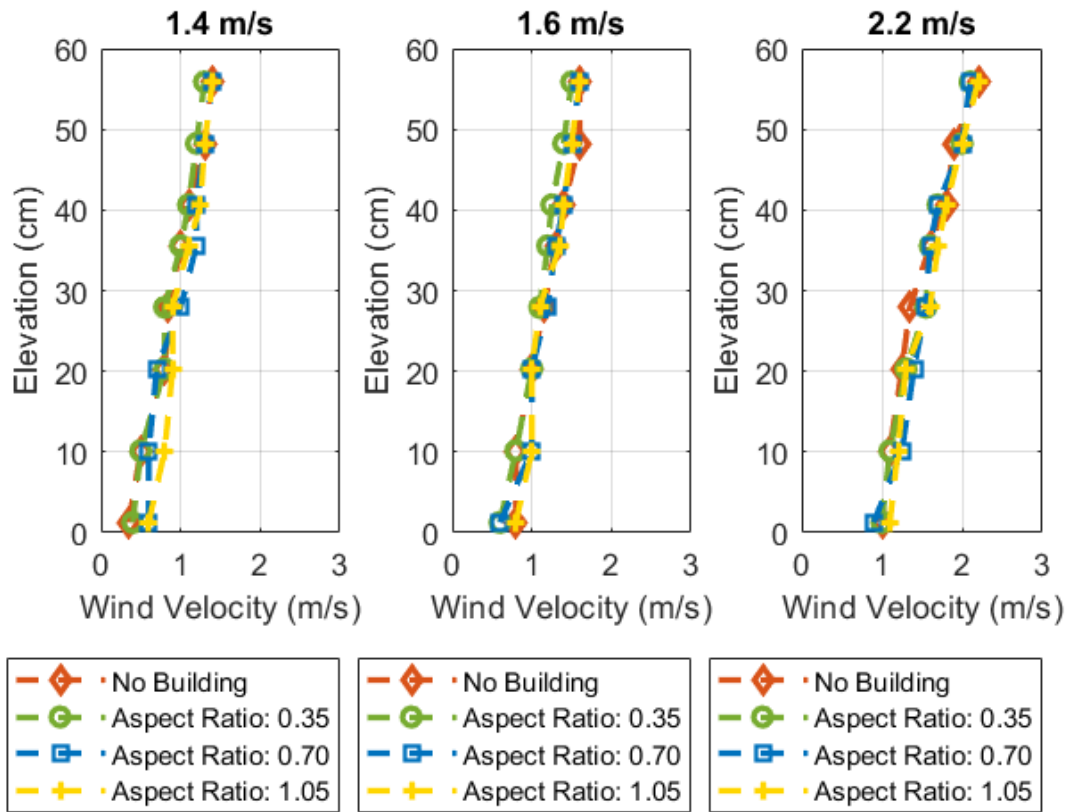


Figure 4.2-1 Wind profiles for different free stream velocities and different aspect ratios.

4.2.2. Concentrations

PM concentration decreased with the presence of buildings, and it tended to decrease further with greater aspect ratios, as shown in Figure 4.2-2. PM concentration differences among the different aspect ratios became less when dust sensors were further away from the centerline. Similar to the experiment without any buildings, PM concentration decreased with a higher free stream velocity.

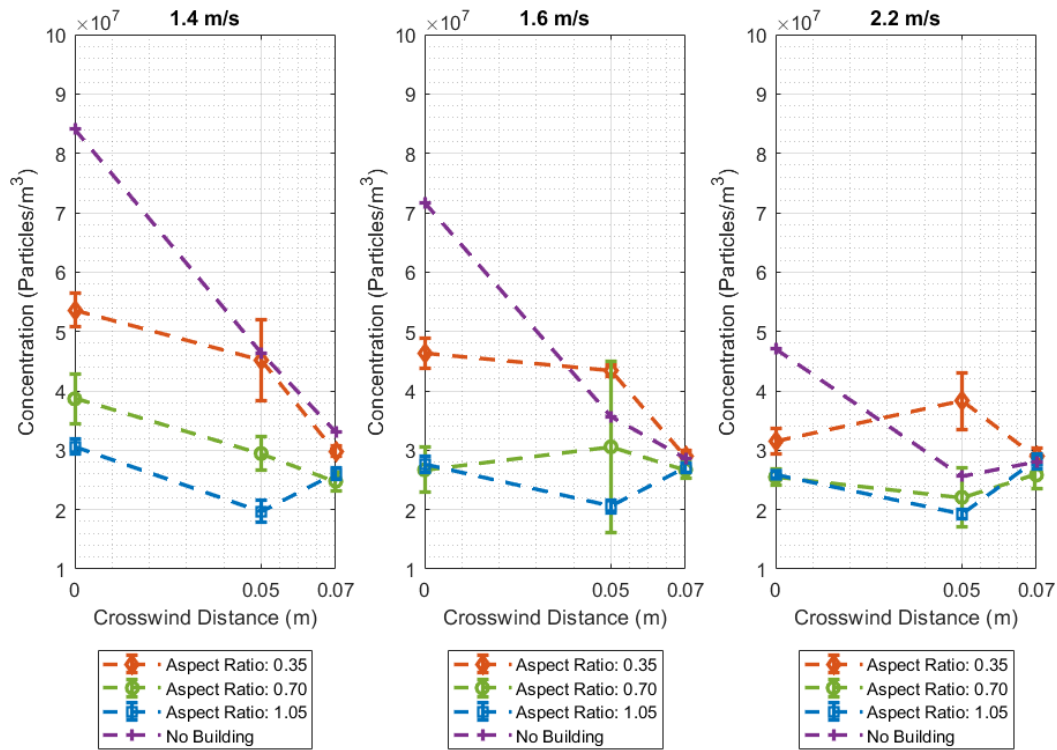


Figure 4.2-2 PM concentrations of open field and street canyons of different aspect ratios.

4.3. CFD Simulation

4.3.1. Model Calibration: Wind Profiles

Wind profiles obtained from the wind tunnel experiment were introduced at the inlet of the fluid domain. The absolute wind velocity deviation of each wind profile from the corresponding experimental wind profile, as shown in Figure 4.3-2, was within 0.1 m/s, except for the elevation of 1.27 m, at which the

deviations could be as high as 0.7 m/s in the inlet profile. The deviation near the ground surface resulted from the setup of computational grids, as ANSYS® FLUENT imposes the velocity value from the profile file at the nearest cell, if it is introduced at the boundary⁴⁵. However, the size of the lowest cell at the domain inlet is 5 m instead of 1.27 m, the corresponding elevation of the lowest wind profile data from the wind tunnel experiment. Overall all the profiles were well maintained and the incident profiles largely resembled the wind tunnel experimental wind profiles, so CFD model setups were valid in terms of wind profiles.

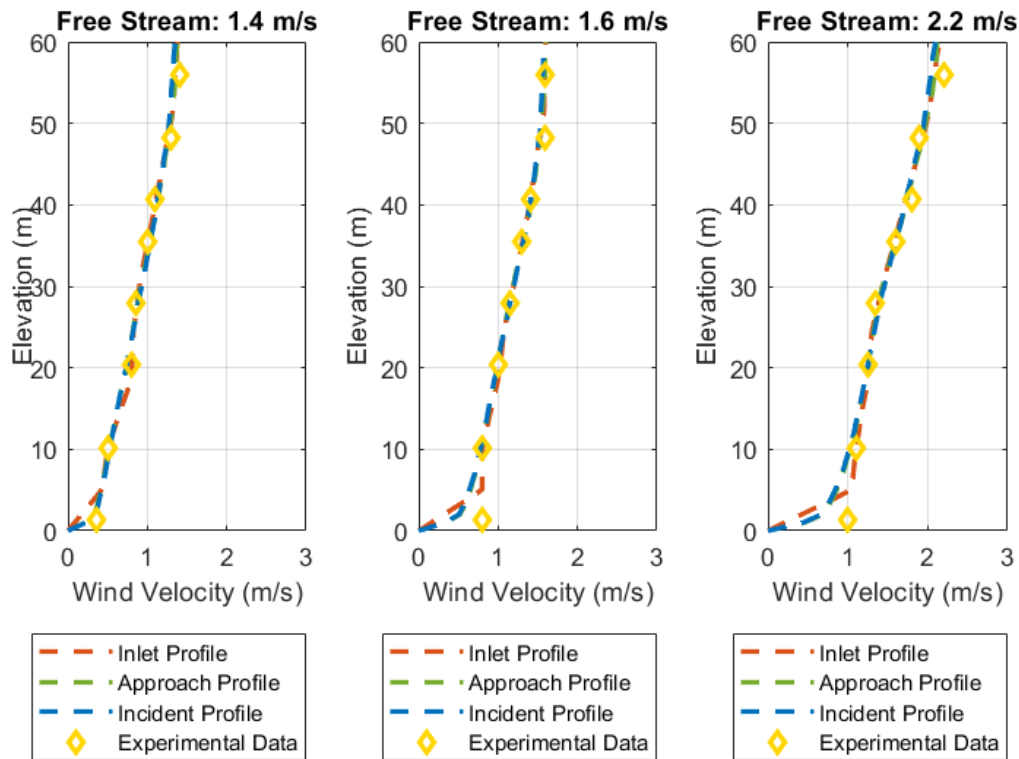


Figure 4.3-1 Wind profiles comparison among inlet profile, approach profile, incident profile, and experimental wind profiles.

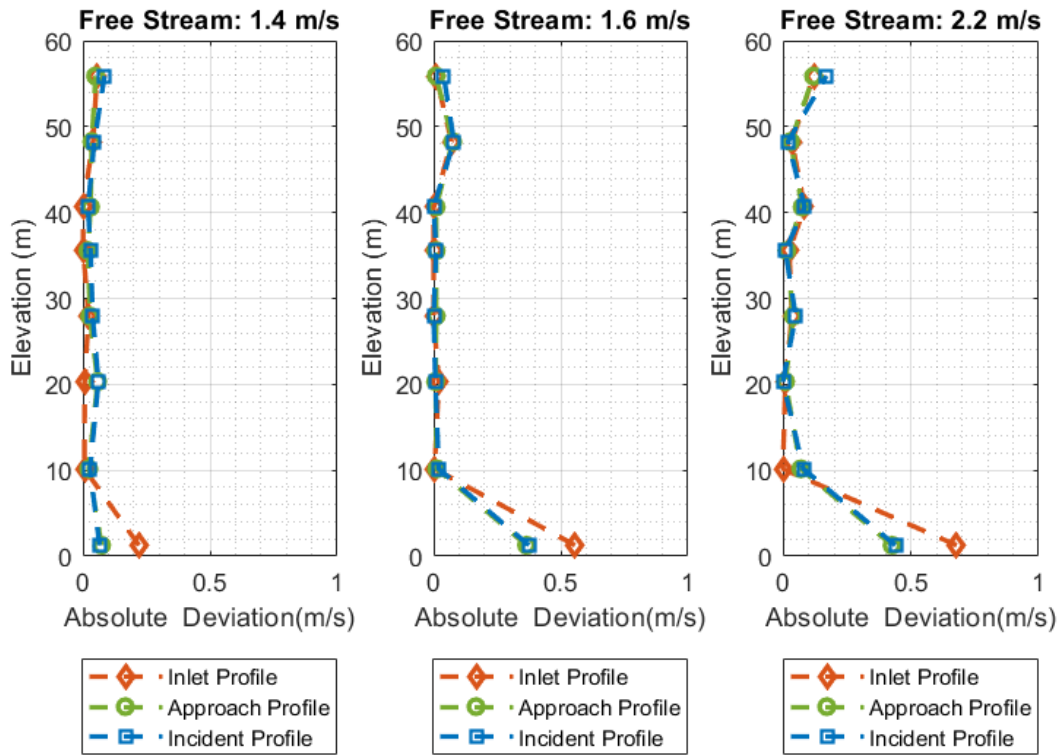


Figure 4.3-2 Absolute wind velocity deviations of inlet profile, approach profile, and incident profile from experimental wind profiles.

4.3.2. Model Calibration: Concentrations

Data from the wind tunnel experiment with buildings and from CFD were quantitatively similar, shown in Figure 4.3-3. The concentration results from CFD simulation were reasonable and expected, as a lower concentration was witnessed with a higher free stream velocity or a greater crosswind distance. The mean deviations from experimental data were 54.9% with a relative standard deviation of 26.6%. In terms of concentrations, CFD model setups were valid.

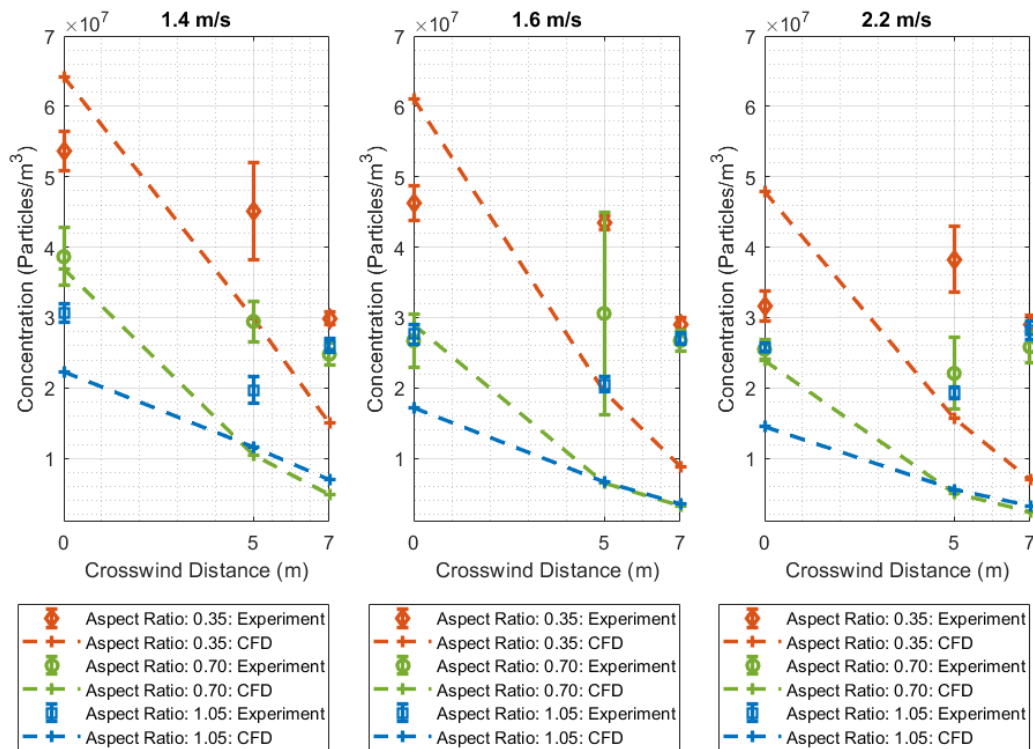


Figure 4.3-3 PM Concentration comparison between CFD simulation and wind tunnel experiment data with street canyon.

4.3.3. PM Concentrations at Breathing Height

Breathing height is defined as the horizontal plane at 1.5 m above the ground. PM concentrations at the breathing height inside the street canyons were obtained solely from CFD simulation. Five percentile concentrations were calculated across all nine setups tested: 50th percentile, 75th percentile, 90th percentile, 95th percentile, and 99th percentile concentrations. Names are assigned to different parts of a generic street canyon, as shown in Figure 4.3-4. There are two channels in a three-dimensional building matrix: The one lies parallel to the wind direction is named “longitudinal”, and the one lies perpendicularly to the wind direction is named “transverse”.

	50 Percentile	75 Percentile	90 Percentile	95 Percentile	99 Percentile
Concentration (particle/m ³)	2.60*10 ⁶	6.99*10 ⁶	2.11*10 ⁷	3.73*10 ⁷	7.88*10 ⁷

Table 4.3-1 Summary of 50 percentile, 75 percentile, 90 percentile, 95 percentile, and 99 percentile concentrations at the breathing level (1.5 m above ground) from the CFD simulation.

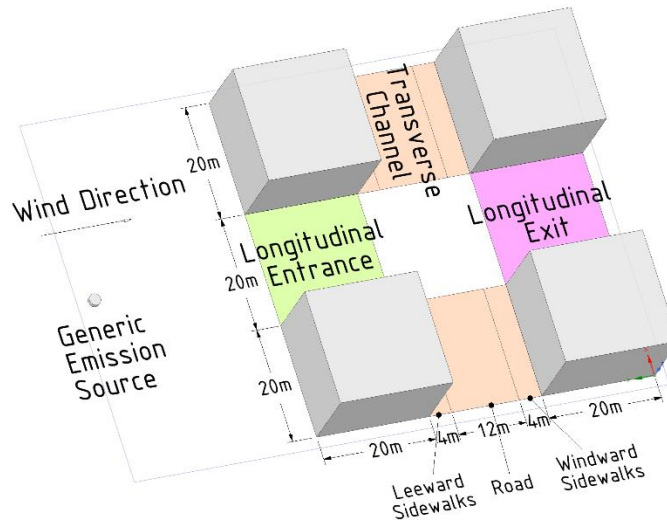


Figure 4.3-4 Graphic illustration of names for different parts of a generic three-dimensional street canyon.

Within the PM concentration contour, as shown in Figure 4.3-5, the lowest concentration that indicated a different color than white was the 50th percentile mark at the breathing height, 2.60×10^6 particles/m³. All the transverse channel except the part overlapping the longitudinal channel registered less than the 50th percentile concentration. The orange color indicated a PM concentration higher than the 90th percentile mark at the breathing height, and the red one indicated a PM concentration higher than the 95th percentile mark. Over 90th percentile concentrations were witnessed at the longitudinal entrance under all setups, and a lower aspect ratio, such as 0.35, resulted in penetration of PM with higher than the 90th percentile concentration.

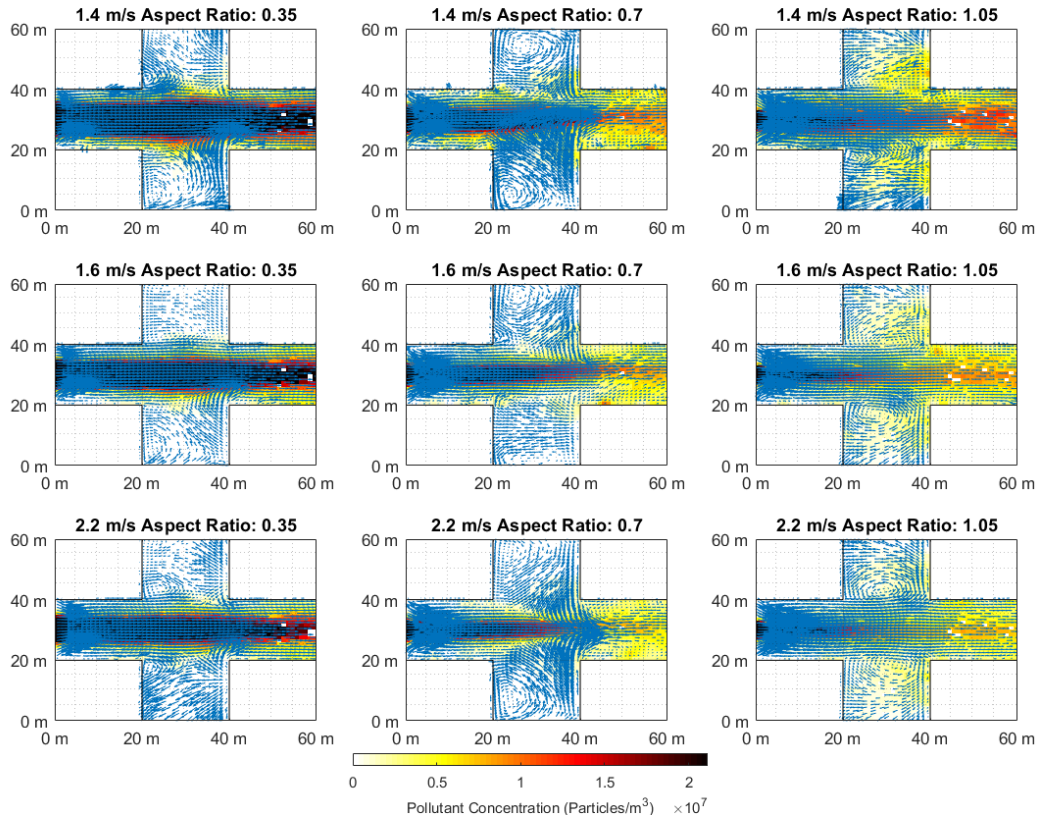


Figure 4.3-5 PM concentration contour and wind velocity vectors at the breathing height from CFD simulation with wind coming from the left. “Orange” indicates concentration higher than the 90th percentile concentration, 2.11×10^7 particles/m³. “Red” indicates concentration higher than the 95th percentile concentration, 3.73×10^7 particles/m³.

The transverse channel registered lower PM concentrations on average than the longitudinal entrance and the longitudinal exit, as shown in Figure 4.3-6. The mean PM concentration in the longitudinal entrance and the longitudinal exit decreased with greater aspect ratio and higher free stream wind velocity. The trend is expected, as a greater aspect ratio or a higher free stream wind velocity resulted in a higher wind velocity within the longitudinal channel and more PM was carried towards the street canyons. However, the mean PM concentration in the transverse channel decreased with greater aspect ratio. Such phenomenon can be explained by reduced localized ventilation capacity due to street canyons with greater aspect ratio⁹.

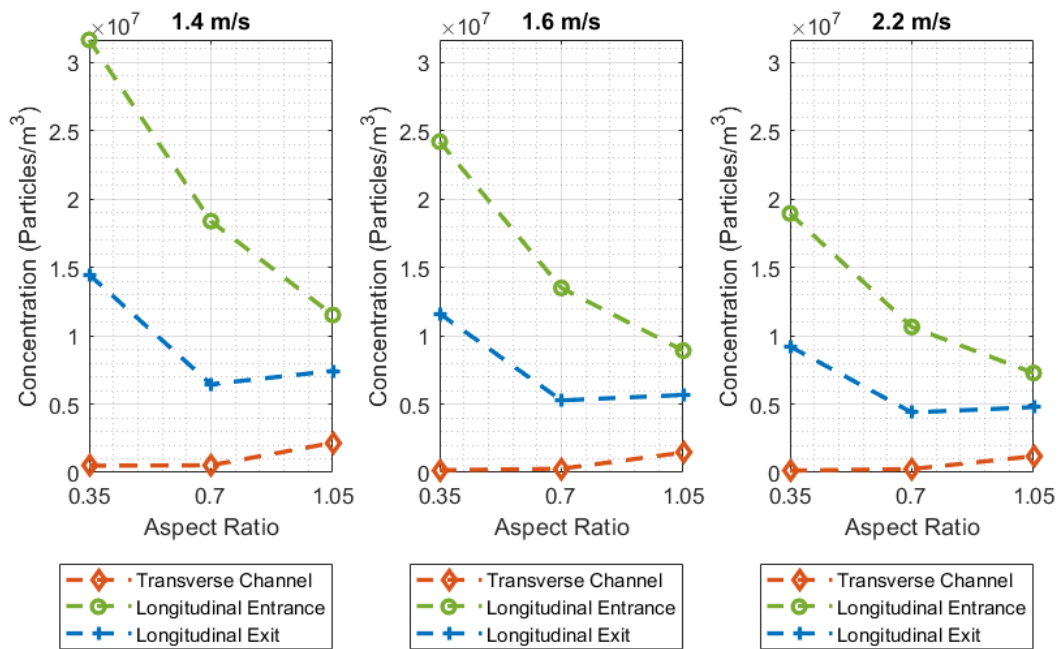


Figure 4.3-6 Mean PM concentrations in the transverse channel, the longitudinal entrance, and the longitudinal exit at the breathing height

Within the transverse channel, as shown in Figure 4.3-7, the leeward sidewalks registered lower PM concentration than the windward sidewalk and the transverse road. The PM concentration increased with greater aspect ratio but decreased with higher free stream wind velocity in all regions. A higher aspect ratio deteriorated air ventilation capacity, hence higher PM concentration, whereas a greater free stream wind velocity induced more dilution, hence lower PM concentration.

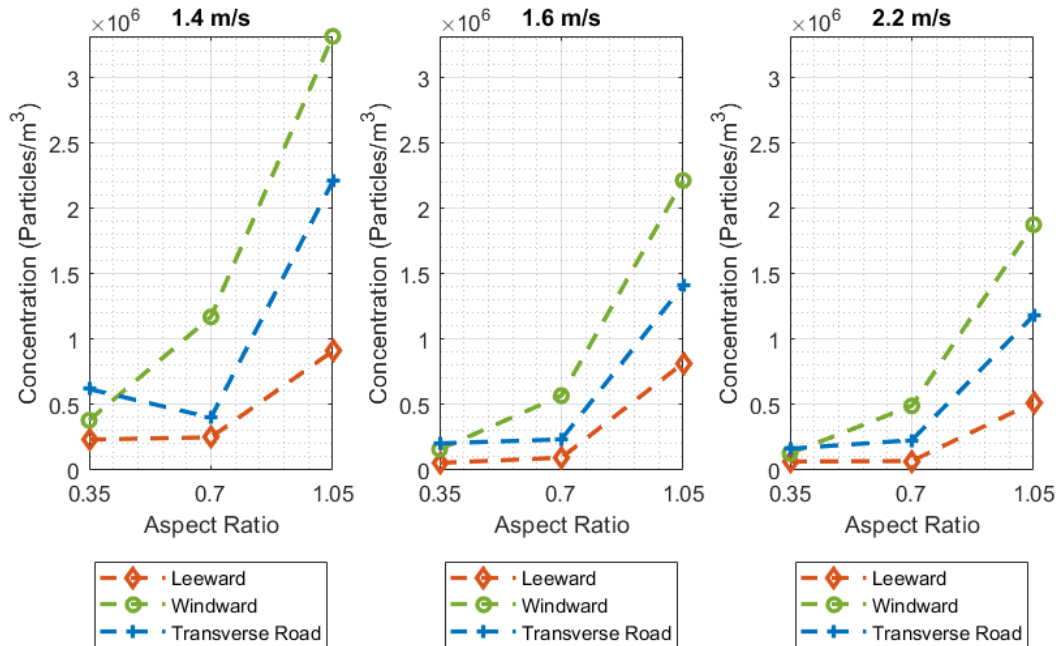


Figure 4.3-7 Mean PM concentration at the leeward sidewalk, the windward sidewalk, and the transverse road at the breathing height.

Within the leeward sidewalk, as shown in Figure 4.3-8, the lowest PM concentration could be found at the transverse exits. PM concentration decreased with greater crosswind distance, but the concentration was considerably higher at the transverse exits when the aspect ratio was 1.05 than those when the aspect ratios were 0.35 and 0.70.

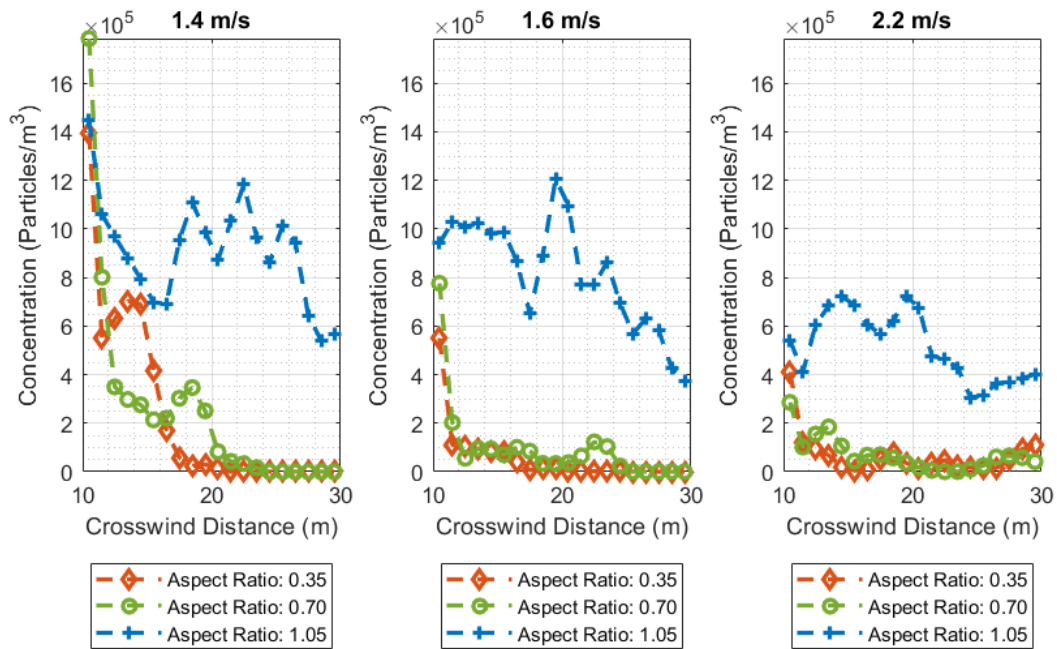


Figure 4.3-8 Mean PM concentration within the leeward sidewalk. A crosswind distance of 0 m is at the longitudinal centerline, and a crosswind distance of 30 m is at the transverse exit.

4.3.4. PM Concentrations along Building Façades

This section shows PM concentration results at the façade surfaces with access to the longitudinal channel and the transverse channel and at the roofs. The façades not facing the central intersection are excluded from consideration in the project, as they all experience extremely low PM concentrations in this scenario. The color scale assigned to particle concentrations is identical in Figure 4.3-9, Figure 4.3-10, Figure 4.3-11, Figure 4.3-12, and Figure 4.3-13, but is different from the one at the breathing level shown in Figure 4.3-5. The lowest concentration that indicates a different color than white in the PM concentration contours is the 50th percentile concentration at the breathing level, 1.54×10^6 particles/m³.

	50 Percentile	75 Percentile	90 Percentile	95 Percentile
Concentration (particles/m ³)	1.54*10 ⁶	4.38*10 ⁶	7.78*10 ⁶	1.08*10 ⁷

Table 4.3-2 Summary of 50 percentile, 75 percentile, 90 percentile, 95 percentile, and 99 percentile concentrations at building façade surfaces from CFD simulation.

A significant portion of the leeward façade registered lower than the 50th percentile concentration overall, except sparse parts located near the longitudinal entrance, as shown in Figure 4.3-9. However, the windward façades could witness noticeable parts with higher than the 50th percentile concentration near the longitudinal channel, shown in Figure 4.3-10. A greater portion of the leeward façades and the windward façades were affected by PM with noticeable concentrations with a greater aspect ratio, as the local ventilation capacity was weakened. However, a higher free stream wind velocity encouraged pollutant dilution, hence a reduced fraction of the façade being affected.

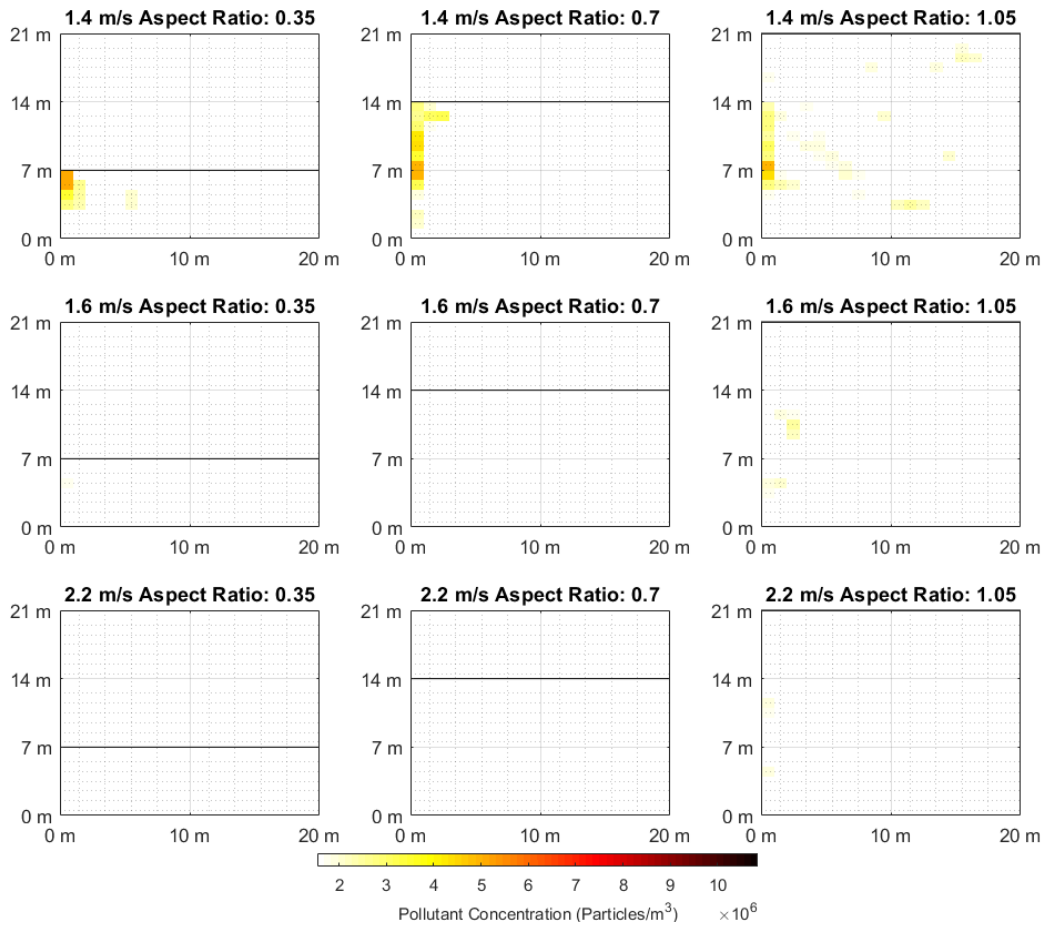


Figure 4.3-9 PM concentration contour at the leeward façade surfaces of the transverse channel with wind coming out of the page. The longitudinal channel is to the left of the individual image.

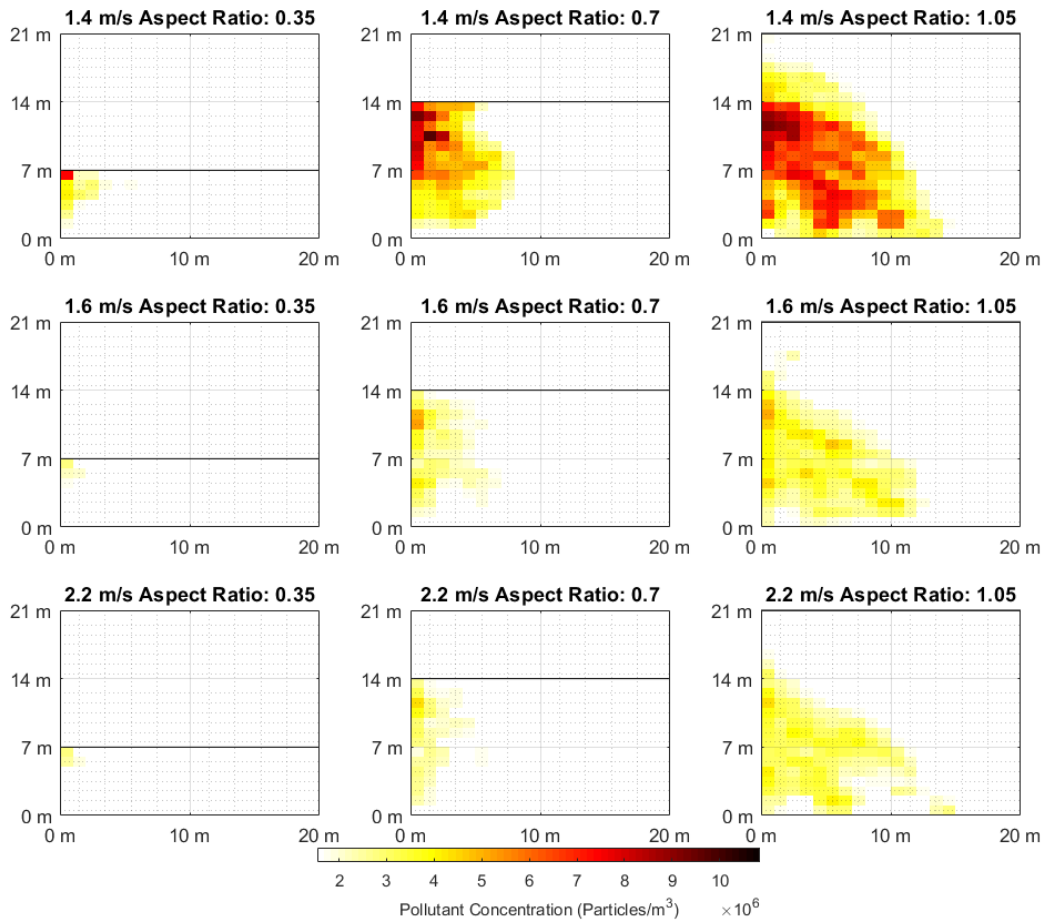


Figure 4.3-10 PM concentration contour at the windward façade surfaces of the transverse channel with wind coming into the page. The longitudinal channel is to the left of the individual image.

At the longitudinal entrance façades, as shown in Figure 4.3-11, no higher than the 50th percentile concentration was registered until it was further downwind from the front edge of the buildings. Nonetheless, most of the longitudinal exit façades were subject to higher than the 75th percentile concentration, as shown in Figure 4.3-12, as PM managed to disperse transversely with more traveling time. Similar to the leeward façades and the windward façades, a greater aspect ratio intensified the severity of pollution in terms of affected areas and PM concentrations, whereas a higher free stream wind velocity could reverse the previous process by diluting PM.

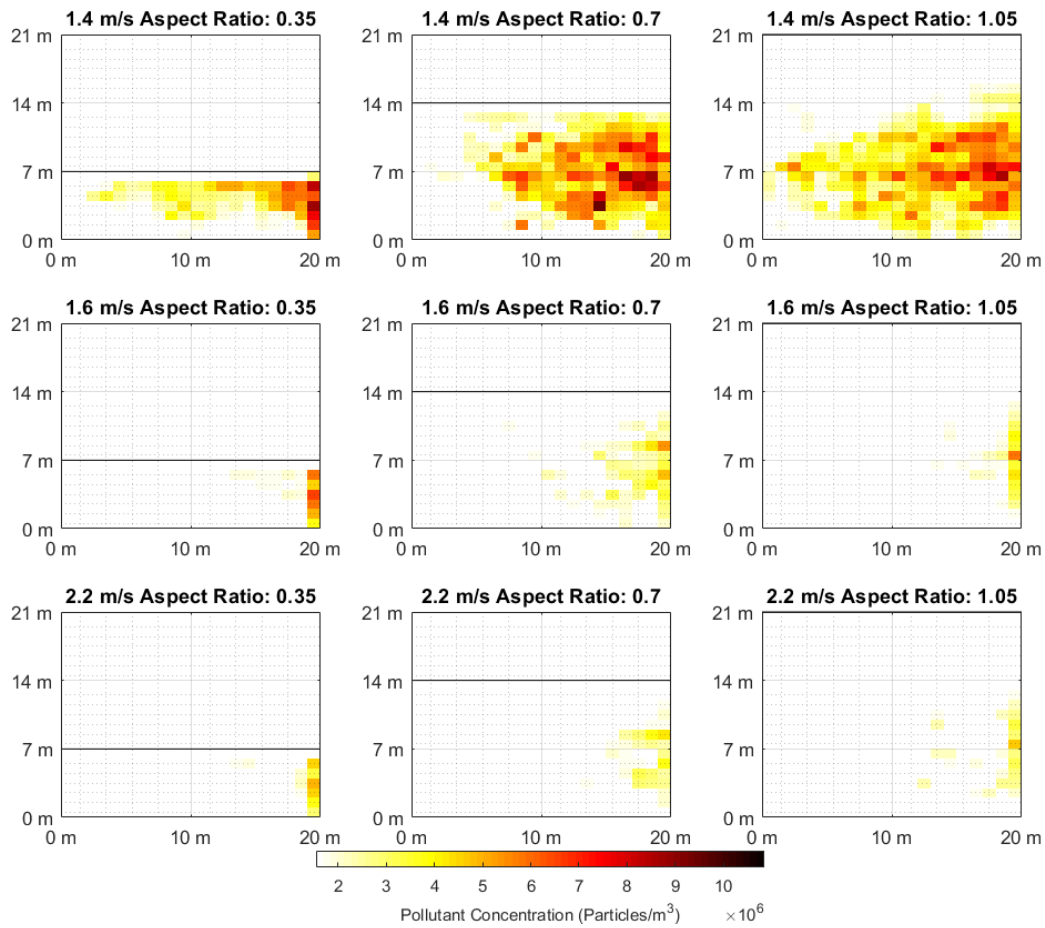


Figure 4.3-11 PM concentration contour at the façade surfaces of the longitudinal entrance with wind coming from left. The transverse channel is to the right of the individual image.

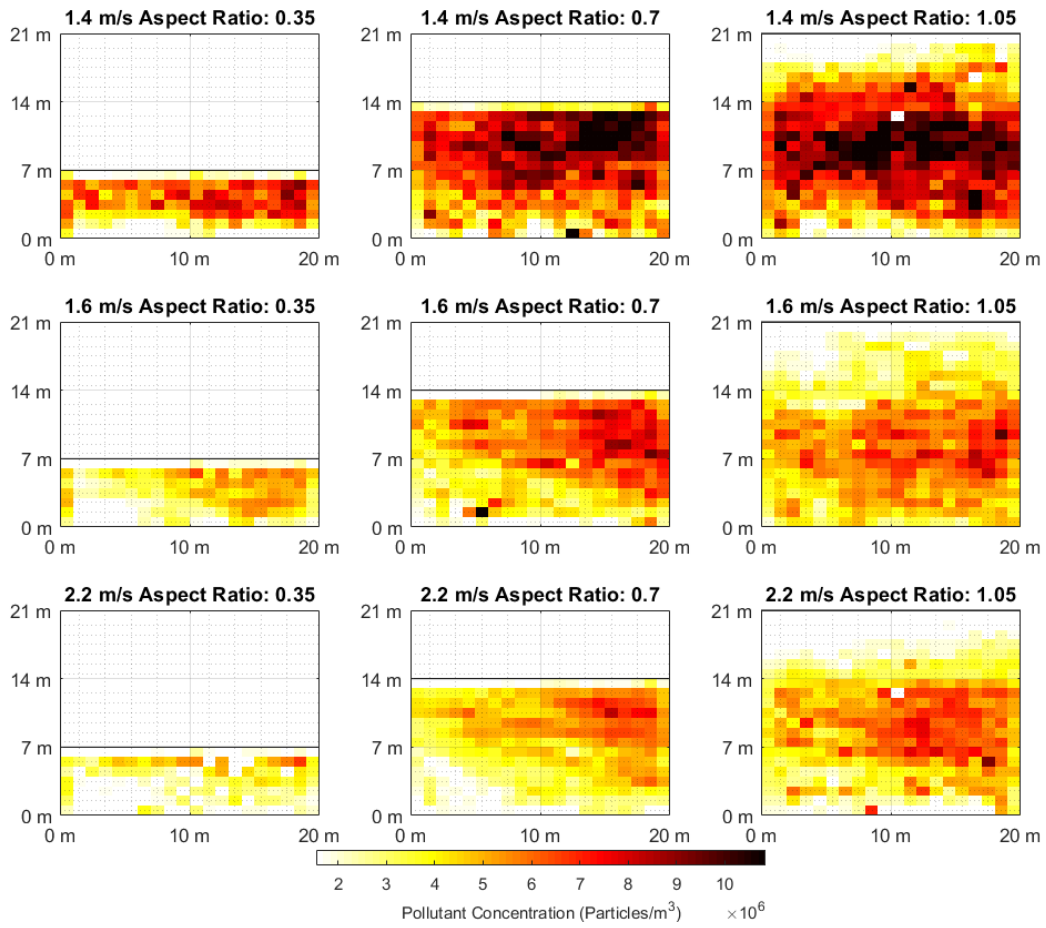


Figure 4.3-12 PM concentration contour at the façade surfaces of the longitudinal exit with wind coming from the left. The transverse channel is to the left of the individual image.

Roofs did not have significant portion with higher than the 50th percentile concentration, as shown in Figure 4.3-13. The only places with higher than 50th percentile concentration were located near the longitudinal exit, and it agreed with Figure 4.3-11 and Figure 4.3-12.

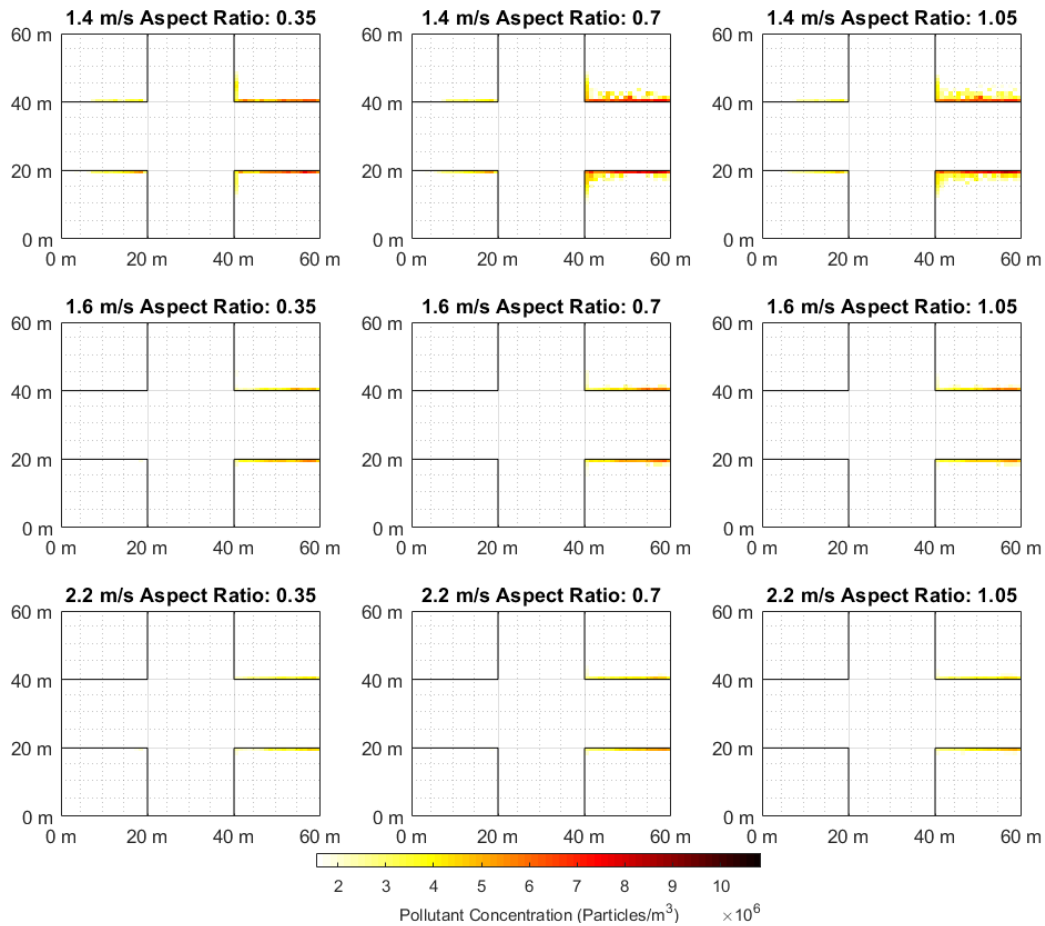


Figure 4.3-13 PM Concentration contour at the roofs with wind coming from the left.

When free stream wind velocities and locations of vertical façades (the leeward façades, the windward façades, the longitudinal entrance façades, and the longitudinal exit façades) are taken out of consideration, a map with PM concentration categorically labelled can be generated as shown by Figure 4.3-14. Therefore, for any vertical façade with access to the internal intersection, the bottom region within 1 m to the ground and the top region within 1 m to the roof had an expected PM concentration less than the 50th percentile mark, 1.54×10^6 particles/m³.

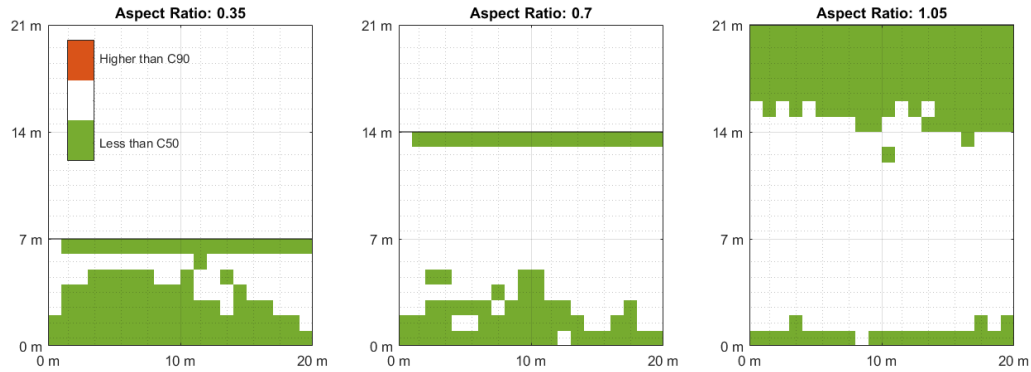


Figure 4.3-14 PM concentration highlighted map of any vertical façade surface regardless of wind velocity and wind direction. Locations with concentration below $1.54 \cdot 10^6$ particles/m³ (the 50th percentile concentration) are labeled green and those with concentration above $1.08 \cdot 10^7$ particles/m³ (the 95th percentile concentration) are labeled orange.

Likewise, when free stream wind velocities and orientations are also taken out of consideration for roofs, the entire area of any roof has an expected PM concentration less than the 50th percentile mark, as shown in Figure 4.3-15.

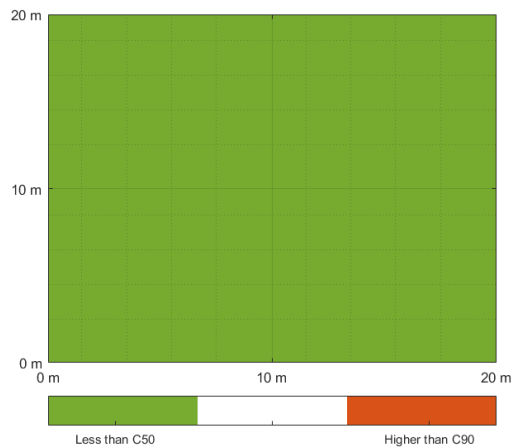


Figure 4.3-15 PM Concentration highlighted map of the roof regardless of wind velocity and wind direction. Locations with concentration below $1.54 \cdot 10^6$ particles/m³ (the 50th percentile concentration) are labeled green and those with concentration above $1.08 \cdot 10^7$ particles/m³ (the 95th percentile concentration) are labeled orange.

When the top 1 m of any vertical façade surface, the bottom 1 m of any vertical façade surface, and the roof are compared to the remaining façade surface in terms of PM concentrations, the former ones had up to 59.9%, 60.8%, 17.3% of the PM concentration at the latter on average, as shown in Figure 4.3-16.

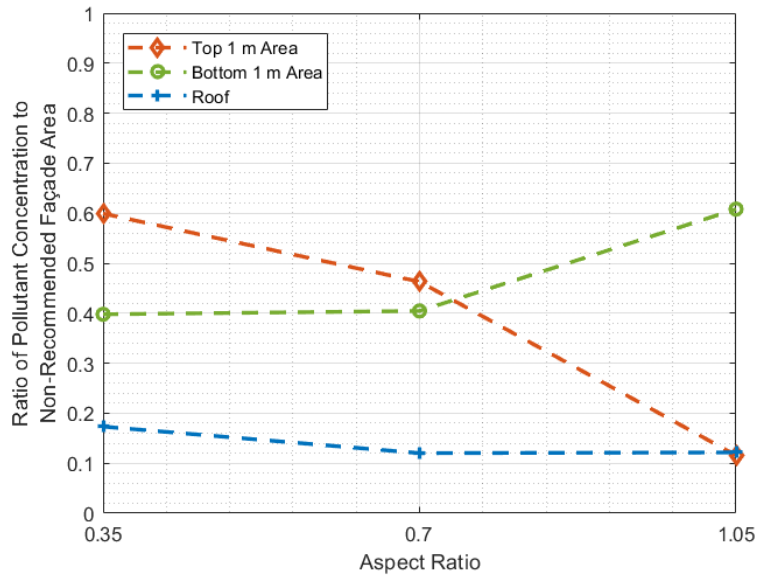


Figure 4.3-16 Ratio of mean PM concentrations at the top 1 m and bottom 1 m of any vertical façade surface and the roof to those at the remaining façade surface.

5. Discussion

The aim of this study is to predict PM dispersion in a three-dimensional street canyon with a continuous point source outside the canyon, so that informed guidance can be provided to pedestrians to move to the lowest risk locations and building ventilation intakes can be designed to minimize uptake of PM from the environment. Since the time between the beginning of a PM release and the arrival of PM in this model scenario is less than 1 min, during which pedestrians might not be able to take other actions than moving to a less affected place, these results can usefully aid the development of emergency response procedures to reduce impacts on the local population.

5.1. Similarity between Wind Tunnel Experiment and CFD Simulation

Overall, the concentrations obtained from the CFD simulation were qualitatively similar to those from the wind tunnel experiment, even though the configurations with aspect ratios of 0.70 and 1.05 underestimated pollutant concentrations as shown in Figure 4.3-3. The mean deviation from the wind tunnel experimental data was 54.9% with a standard deviation of 26.6%.

The overall trend found in the wind tunnel experiment was successfully replicated in the CFD simulation, as a lower pollutant concentration can be found with a greater aspect ratio, a greater free stream wind velocity, and a greater crosswind distance. A similar phenomenon could also be found in Figure 4.3-5, as the area with higher than the 90th percentile concentration shrank with a higher aspect ratio. The relation between PM concentration and aspect ratio can be surprising and contradictory to the results in the literature, as Oke, Chang and Meroney, and Meroney et al. suggested that a greater aspect ratio typically resulted in lower local ventilation capacity due to vortices formed within the canyon between the leeward façade and the windward façade, hence higher pollutant concentration, as shown in Figure 4.3-9 and Figure 4.3-10^{8,9,14}. Nonetheless, the wind tunnel experiment of this study had street canyons designed

with a longitudinal channel aligning with the emission source and placed three dust sensors in the longitudinal channel, so no leeward façade and windward façade existed for the sensors and such absence facilitates wind traveling through the longitudinal channel.

5.2. Prediction of PM Concentration with Decay Only

Figure 4.1-6 and Figure 4.1-7 showed that the transport case of *Dispersion Only* could decrease PM concentration far greater than the case of *Decay Only* at the centerline ground, but the magnitude of PM concentration change due to *Decay Only* could be unreliable, as mentioned in Section 3.1.7, because the same value of the decay coefficient, k , was used in the cases of *Decay Only* (Equation 8) and *Dispersion and Decay* (Equation 2 with y and z being 0). However, k was initially estimated from the modified Gaussian plume model, which accounted for both dispersion and decay. The count density of PM in the case of *Decay Only* should outnumber that in the case of *Dispersion and Decay*, because the dispersion was responsible for the crosswind and vertical movement of PM and therefore decreased PM concentration as shown in Figure 4.1-6. The decay accounted for evaporation and coalescence. Regarding evaporation, a greater count density of PM should raise local humidity and hence lower evaporation rate, resulting in less value of k ⁴⁶. Regarding coalescence, however, PM with a greater count density were more likely to collide with each other, resulting in a higher coalescence rate and greater value of k . Therefore, k estimated from the modified Gaussian plume model could be inaccurate for the case of *Decay Only*.

5.3. Evacuation during Release Emergency

If an accidental PM release occurs outside the street canyon with PM or volatile organic compounds (VOC) with high molecular weight and wind is blowing towards the street canyon, pedestrians should be evacuated to the leeward side of the transverse exits.

The entire street canyons were divided into three distinct regions, the longitudinal entrance, the longitudinal exit, and the transverse channel, as shown in Figure 4.3-4. In Figure 4.3-6, the transverse channel registered the lowest pollutant concentration, and the longitudinal entrance registered the highest pollutant concentration among the three. Figure 5.3-1 shows that the longitudinal entrance and the longitudinal exit had a PM concentration at least 430% and 242% higher than the transverse channel on average, respectively.

Lower pollutant concentration detected in the transverse channel on average was anticipated. The wind channeled pollutants through the longitudinal entrance and the longitudinal exit without any burden. Therefore, accumulation of pollutants within the transverse channel could be relatively difficult when negative pressure created at the longitudinal channel due to higher local wind velocity forced air to move towards the middle of the intersection.

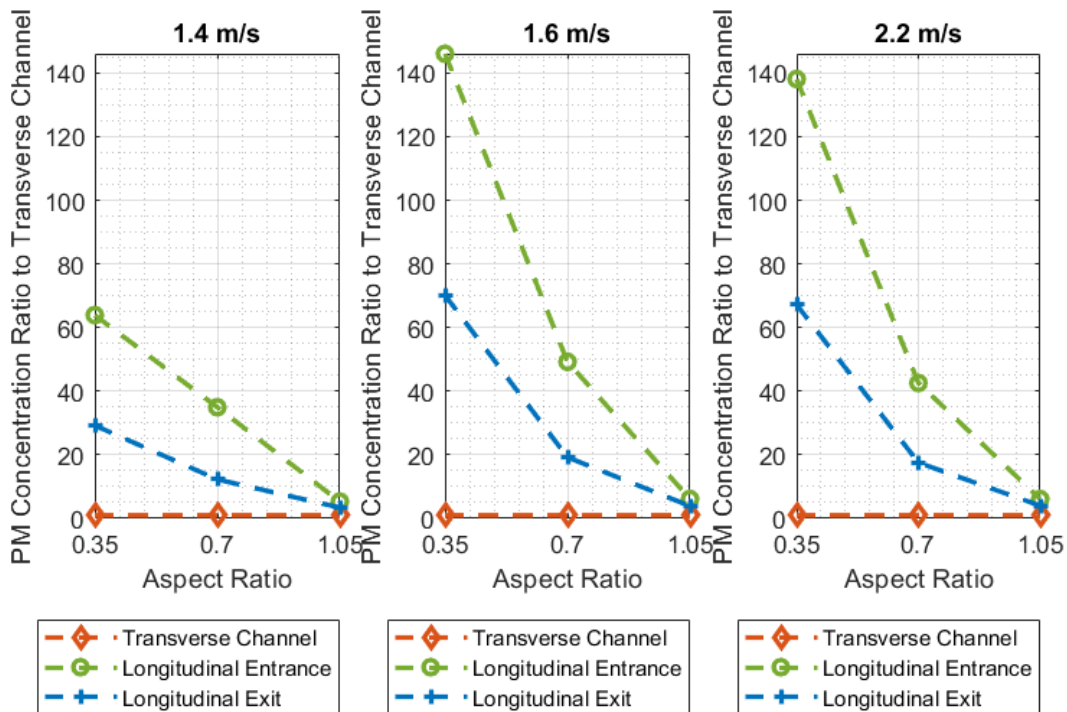


Figure 5.3-1 Ratio of PM concentrations at the longitudinal entrance and the longitudinal exit to those at the transverse channel at the breathing height.

Furthermore, the transverse channel could be divided into the leeward sidewalks, the windward sidewalks, and the transverse road. The leeward sidewalks and the windward sidewalks referred to the region that was within 4 m to the leeward façade and the windward façade, respectively. The transverse roads were 12 m wide covering the region in between the two sidewalks. The wind tunnel studies in the past by Chang and Meroney, Kastner-Klein and Plate, and Meroney et al. mounted sampling ports onto the façades^{8,11,14}. Others placed them inside the canyon¹². The CFD studies could be more versatile, as they could freely choose where to place sampling ports^{13,15-17}. Both façades and sidewalks will be referred to as “sidewalks” in this section when PM concentration is discussed.

From the CFD simulation, Figure 4.3-7 shows that the PM concentration within the transverse channel at the breathing height was the highest at the windward sidewalks and was the least at the leeward sidewalks, regardless of aspect ratio and free stream wind velocity. Additionally, the comparison between the leeward façade surfaces (Figure 4.3-9) and the windward façade surfaces (Figure 4.3-10) indicates that the windward surface was more impacted by pollutant than its opposite side. Figure 5.3-2 shows that the windward sidewalks and the transverse roads could have a PM concentration at least 63% and 60% higher than that of the leeward sidewalks at the breathing height.

This finding contradicts with the work done by Chang and Meroney, as they suggested that the leeward sidewalks could have up to ten times the concentration of the windward sidewalks near the ground and have up to four times the concentration near the roof when the aspect ratio was 1.0⁸. A main difference between this study and the work by Chang and Meroney was the location of the point source, as the former placed it outside the street canyons but the latter placed it between the leeward façade and the windward façade⁸. At the ground level, there should exist some vortices that moved from the windward façade towards the leeward façade as a result of wind reflected from the windward façade, hence a higher

pollutant concentration in the work by Chang and Meroney⁸. Despite the existence of the vortices, pollutants could hardly interact with them if they are not continuously generated there, and pollutants carried by wind from outside the street canyons are likely to accumulate at the windward sidewalks after contact with the windward façade.

Therefore, for any street canyons that consist similar geometries as those modeled here, it is recommended that pedestrians move to the area labelled green in Figure 5.3-3, which is the leeward sidewalks of the transverse channel.

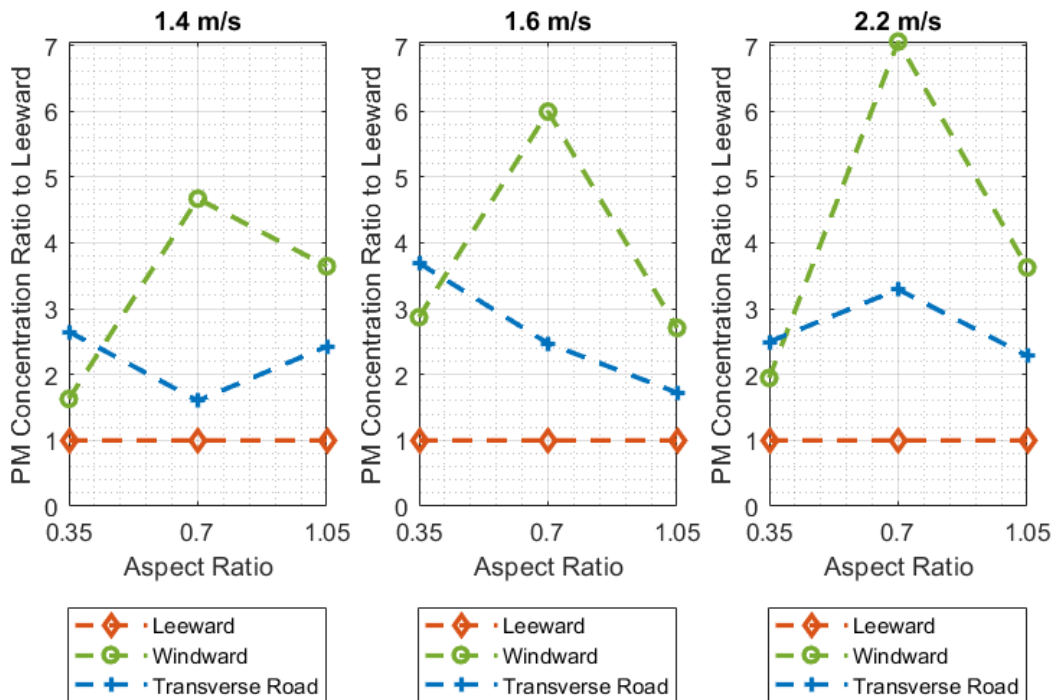


Figure 5.3-2 Ratio of PM concentrations at windward sidewalks and transverse road to those at leeward sidewalks at the breathing level (1.5 m above the ground).

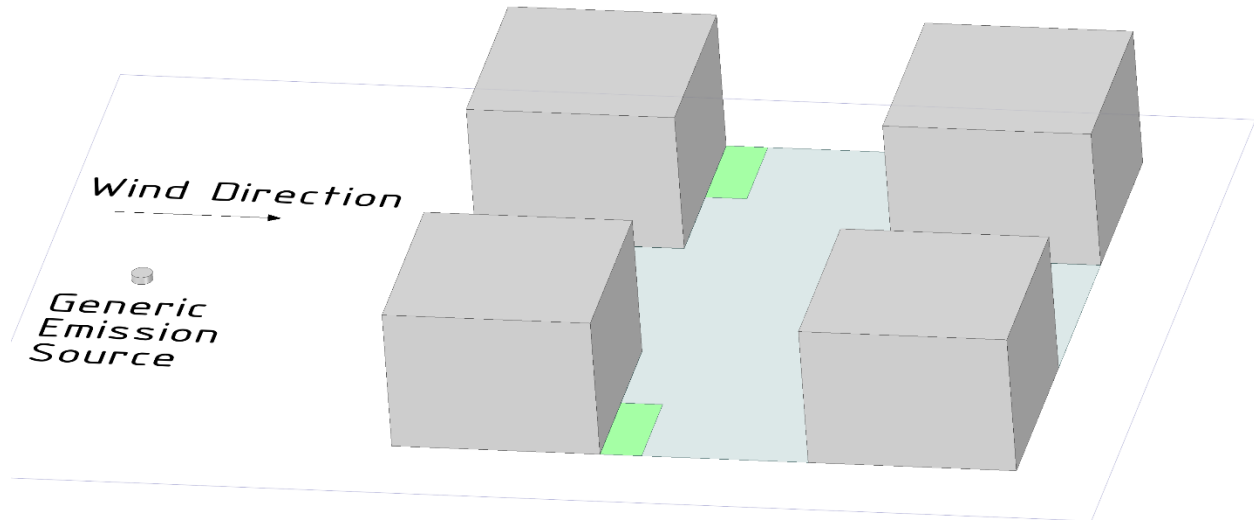


Figure 5.3-3 Recommended exterior shelter areas (green) for pedestrians during an accidental release from a site on the left.

5.4. Ventilation Air Intakes during Release Emergency

Higher pollutant concentrations can be located at both leeward façade and windward façade near the longitudinal channel, as shown in Figure 4.3-9 and Figure 4.3-10, since the emission source was closer to that part of the façades. The leeward façade had a larger area with PM concentration less than the 50th percentile mark, 1.54×10^6 particles/m³ with all aspect ratios and free stream wind velocities. In Figure 5.4-1, the ratio of area less than the 50th percentile concentration in the leeward façade to the windward façade increased with greater aspect ratio but decreases with higher free stream wind velocity.

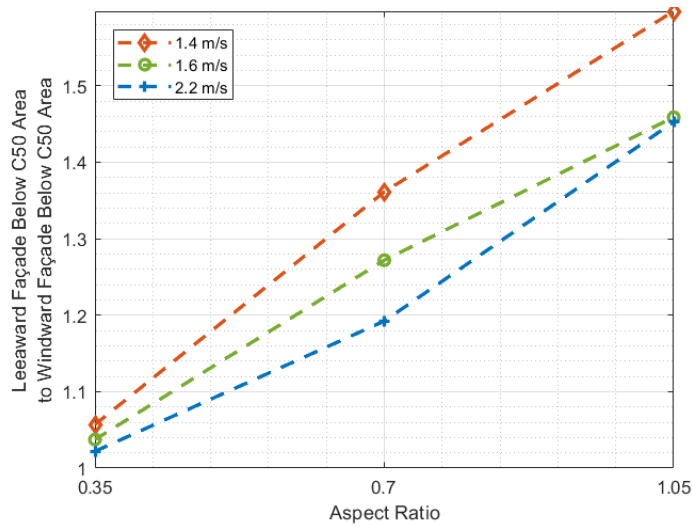


Figure 5.4-1 Ratio of area less than the 50th percentile concentration in the leeward façades to that in the windward façades.

In the longitudinal entrance, as shown in Figure 4.3-11, the area with higher than the 50th percentile concentration was located near the transverse channel, whereas most of the area in the longitudinal exit, as shown in Figure 4.3-12, was subject to higher than the 50th percentile concentration. Additionally, Figure 5.4-2 shows that the area with concentration below the 50th percentile mark in the longitudinal entrance was at least three times that in the longitudinal exit. The main reason was that pollutants had more time to disperse transversely due to the longitudinal exit being downwind to the longitudinal entrance, and no-slip wall treatment in the CFD simulation on street canyons façade surfaces could slow down pollutants movement once pollutants were in the vicinity of street canyons³⁷.

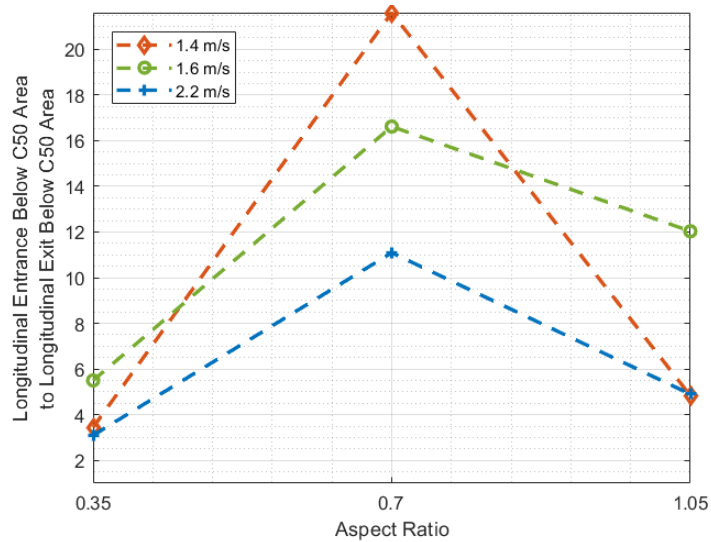


Figure 5.4-2 Ratio of area with less than the 50th percentile concentration in the longitudinal entrance to that in the longitudinal exit.

Figure 4.3-14 and Figure 4.3-15 show that the area with expected pollutant concentration less than the 50th percentile mark was located on the roofs as well as the top and the bottom 1 m of any façade surface in any street canyon with four buildings. The overall area is labelled green in Figure 5.4-3. It is reasonable that the roofs and the top 1 m of any façade had less than the 50th percentile concentration, because of the presence of buildings accelerating local wind velocity in the channel along the wind direction. The result that the bottom 1 m of any façade surface had less than the 50th percentile concentration is also reasonable, because pollutants were brought up in the air when they arrived in the street canyons, as shown in Figure 4.3-9, Figure 4.3-10, Figure 4.3-11, and Figure 4.3-12, which have areas with higher pollutant concentration aloof from the ground.

Therefore, for any building that is between 0.35 and 1.05 in aspect ratio, it is suggested that new ventilation air intakes be placed in the green area shown in Figure 5.4-3, which is the roofs and the top and the bottom 1 m of any façade surface with access to the internal intersection. If ventilation air intakes

are already installed in the orange area shown in Figure 5.4-3, they should be closed during an accidental PM release to ensure air quality inside the buildings.

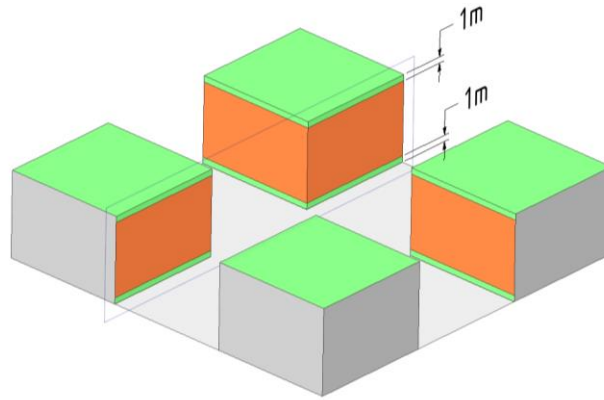


Figure 5.4-3 Recommended area (green) and compromised area (orange) for ventilation air intakes installation in a generic three-dimensional street canyon

5.5. Limitations

There are three main limitations in the study that can be improved in the future.

First, the pollutant transport in the urban environment is essentially transient, as suggested by Chang and Meroney, but the standard $k - \epsilon$ turbulence model used in the CFD simulation is steady-state instead⁸. Even though a transient particle tracking scheme was enabled in the Discrete Phase Model (DPM) of the CFD simulation, the steady-state approach in the turbulence model cannot always guarantee prediction accuracy. Simulation of pollutant dispersion with transient calculation can make prediction applicable to the scenario of instantaneous release.

Second, the size of computational grids in the CFD simulation may not be fine enough. As suggested by Franke et al. and Franke and Baklanov, it is essential to have fine computational grids, so that most of the physical phenomenon can be captured^{34,35}. However, the software used in the CFD simulation, ANSYS® FLUENT imposes a limit of 512000 cells in fluid domain for academic license users. The smallest cell was 1 m in street canyons and the number of cells was barely below the limit. If the street canyons were built even larger, the entire fluid domain would become larger accordingly, and the number of cells would exceed the limit, unless the size of cells were to be compromised.

Third, the evacuation guideline in Section 5.3 and the ventilation air intakes installation guideline in Section 5.4 may not be inapplicable if the actual street canyons in question is out of the range of aspect ratios tested in this study (i.e. from 0.35 to 1.05). A much smaller aspect ratio or a much greater aspect ratio will be likely to develop an entirely different flow pattern in the street canyons affecting the resulting concentrations of pollutants. The field study conducted by De Paul and Shieh showed that multiple vortices could be generated in a deep two-dimensional street canyon⁴⁷. Oke further commented that the phenomenon of the leeward side having higher pollutant concentration than the windward side with one vortex could be reversed when two vortices in the vertical direction exist simultaneously in the street canyon⁹. Despite two-dimensional street canyons in the studies by DePaul and Shieh as well as Oke, it is a reasonable speculation that three-dimensional street canyons with greater aspect ratios may develop flow patterns completely different from the ones in this study^{9,47}.

5.6. Future Work

A main part of future work lies in wind tunnel studies with building models of a less scaling ratio. Larger building models in the wind tunnel can potentially enable researchers to take measurements at most of the locations that are inaccessible in the wind tunnel with much smaller models.

Regarding pollutants, minerals could be added into the distilled water of the PM generator to increase its visibility to the dust sensors. Studies by Rodes et al. as well as Highsmith, Rodes, and Hardy showed that a much higher indoor particulate mass concentration was detected when distilled water and minerals were used in ultrasonic humidifiers^{42,48}. The addition can be conducive to dust sensors detection accuracy, as the aerosols are not evaporative or subject to coalescence as much as distilled water droplets.

Other parameters that should be tested in the future as experimental variables are wind direction, emission source location, and street canyons with more buildings. Taking wind direction and emission source location into consideration can be conducive to developing guidelines for evacuation routes and ventilation air intakes installation, because both are unknown ahead of an incident. Street canyons with more buildings can also make the study more accurate in the future, as street canyons with mere four buildings in open ground can be rare to find.

6. Conclusion

This study simulated an accidental particulate matter (PM) release scenario of a point emission source outside a three-dimensional street canyon of a two-by-two building matrix with an aspect ratio of 0.35, 0.70, and 1.05 via wind tunnel experiments and CFD simulations. The PM source aligned with a channel named “longitudinal channel” and the other channel was named “transverse channel”. The CFD simulation results indicated that the leeward sidewalks of the transverse exits had the lowest PM concentration at the breathing level. Regarding the building facades with access to the internal intersection, the top 1 m and the bottom 1 m of any vertical façade and the roof had the lowest PM concentration.

Statistically, at the breathing level, the longitudinal channel registered at least a 242% higher PM concentration than the transverse channel, and locations inside the transverse channel other than the leeward sidewalks had at least a 60% higher PM concentration at the leeward sidewalks on average. For building façade surfaces, the top 1 m of any vertical façade surface, the bottom 1 m of any vertical façade surface, and the roof had up to 59.9%, 60.8%, and 17.3% of the PM concentration, respectively, at the rest of the façade surface on average, regardless of wind direction, PM source location, and aspect ratio.

Therefore, in an emergency scenario of accidental release outside the street canyons, pedestrians should be advised to move to the leeward sidewalks of the transverse exits and any building ventilation air intakes should be advised to close if they are not in the top 1 m or the bottom 1 m of any vertical façade or on the roofs. For emergency preparedness and general improvement of indoor air quality, it is suggested that new building ventilation air intakes be installed at the top 1 m and the bottom 1 m of any vertical façade and the roofs in order to make air with low PM concentration available.

For the future work, more complex and detailed urban landscape can be introduced in wind tunnel experiments and new variables should be explored, such as wind direction and emission source location, because it is uncommon to find an actual PM release scenario that has the similar street canyon, wind direction, and emission source location as the one tested in this study.

References

1. Fenger, J. Air pollution in the last 50 years - From local to global. *Atmos. Environ.* **43**, 13–22 (2009).
2. Fuzzi, S., Baltensperger, U., Carslaw, K., Decesari, S., Denier Van Der Gon, H., Facchini, M. C., Fowler, D., Koren, I., Langford, B., Lohmann, U., Nemitz, E., Pandis, S., Riipinen, I., Rudich, Y., Schaap, M., Slowik, J. G., Spracklen, D. V., Vignati, E., Wild, M., *et al.* Particulate matter, air quality and climate: Lessons learned and future needs. *Atmos. Chem. Phys.* **15**, 8217–8299 (2015).
3. Seinfeld, J. H. & Pandis, S. N. Chapter 2: Atmospheric Tracer Constituents. in *Atmospheric Chemistry and Physics: From Air Pollution to Climate Change* 47–48 (John Wiley & Sons, Inc, 2016).
4. Chow, J. C. & Watson, J. G. *Guideline on speciated particulate monitoring. Report prepared for US Environmental Protection Agency, Research Triangle Park, NC, by Desert Research Institute, Reno, NV* (1998).
5. Diffey, B. L. An overview analysis of the time people spend outdoors. *Br. J. Dermatol.* **164**, 848–854 (2011).
6. Dockery, D. & Pope, A. Acute respiratory effects of particulate air pollution. *Annu. Rev. Public Health* **15**, 107–132 (1994).
7. Zhang, Y. W., Gu, Z. L., Lee, S. C., Fu, T. M. & Ho, K. F. Numerical simulation and in situ investigation of fine particle dispersion in an actual deep street canyon in Hong Kong. *Indoor Built Environ.* **20**, 206–216 (2011).
8. Chang, C. H. & Meroney, R. N. Concentration and flow distributions in urban street canyons: Wind tunnel and computational data. *J. Wind Eng. Ind. Aerodyn.* **91**, 1141–1154 (2003).
9. Oke, T. R. Street Design and Urban Canopy Layer Climate. *Energy Build.* **11**, 103–113 (1988).

10. Buonanno, G., Fuoco, F. C. & Stabile, L. Influential parameters on particle exposure of pedestrians in urban microenvironments. *Atmos. Environ.* **45**, 1434–1443 (2011).
11. Kastner-Klein, P. & Plate, E. J. Wind-tunnel study of concentration fields in street canyons. *Atmos. Environ.* **33**, 3973–3979 (1999).
12. Pavageau, M. & Schatzmann, M. Wind tunnel measurements of concentration fluctuations in an urban street canyon. *Atmos. Environ.* **33**, 3961–3971 (1999).
13. Wedding, J. B., Lombardi, D. J. & Cermak, J. E. A wind tunnel study of gaseous pollutants in city street canyons. *J. Air Pollut. Control Assoc.* **27**, 557–566 (1977).
14. Meroney, R. N., Pavageau, M., Rafailidis, S. & Schatzmann, M. Study of line source characteristics for 2-D physical modelling of pollutant dispersion in street canyons. *J. Wind Eng. Ind. Aerodyn.* **62**, 37–56 (1996).
15. Gromke, C., Buccolieri, R., Di Sabatino, S. & Ruck, B. Dispersion study in a street canyon with tree planting by means of wind tunnel and numerical investigations - Evaluation of CFD data with experimental data. *Atmos. Environ.* **42**, 8640–8650 (2008).
16. Assimakopoulos, V. D., ApSimon, H. M. & Moussiopoulos, N. A numerical study of atmospheric pollutant dispersion in different two-dimensional street canyon configurations. *Atmos. Environ.* **37**, 4037–4049 (2003).
17. Huang, H., Akutsu, Y., Arai, M. & Tamura, M. A two-dimensional air quality model in an urban street canyon: Evaluation and sensitivity analysis. *Atmos. Environ.* **34**, 689–698 (2000).
18. Irwin, H. P. A. H. The design of spires for wind simulation. *J. Wind Eng. Ind. Aerodyn.* **7**, 361–366 (1981).
19. Shinyei Corporation of America. *Specification Sheet of PPD42NS*. (2010).

20. DATAQ Instruments. *Using DATAQ . NET Controls in MATLAB* ®. (2016).
21. Ray, M. L., Rogers, A. L. & McGowan, J. G. Analysis of Wind Shear Models and Trends in Different Terrains. *AWEA Wind Power 2005 Conf.* 4–7 (2006).
22. Bechrakis & Sparis. Simulation of the wind speed at different heights using artificial neural networks. *Wind Eng.* 127–136 (2000).
23. Snyder, W. H. Models To the Study of Air Pollution Meteorology. *Boundary-Layer Meteorol.* **3**, 113–134 (1972).
24. Townsend, A. A. *Structure of Turbulent Shear Flow*. (Cambridge University Press, 1956).
25. Meroney, R. N. & Neff, D. E. Reynolds number independence of the wind tunnel simulation of transport and dispersion about buildings. *Unpubl. Intern. Memo.* 21 (1996).
26. Cermak, J. E. & Peterka, J. *Simulation of wind fields over point arguello, California, by wind-tunnel flow over a topographic model. Colorado State Univ Fort Collins Fluid Dynamics and Diffusion Lab* (1966).
27. Hidy, G. M. Adventures in Atmospheric Simulation. *Am. Meteorol. Soc.* **48**, 143–161 (1967).
28. McVehil, G., Ludwig, G. & Sundaram, T. *On the feasibility of modeling small scale atmospheric motions (CAL-ZB-2328P-1)*. (1967).
29. Hanna, S. R., Briggs, G. A. & Hosker, R. P. J. *Handbook on atmospheric diffusion.* **11223**, (1982).
30. Crawl, D. A. & Louvar, J. F. Toxic release and dispersion models. in *Chemical Process Safety: Fundamentals with Applications* 186 (Prentice Hall PTR, 2011).
31. Cushman-Roisin, B. 2.8 Advection and diffusion. in *Environmental transport and fate* 69 (Thayer School of Engineering, Dartmouth College, 2012).
32. Blocken, B., Janssen, W. D. & van Hooff, T. CFD simulation for pedestrian wind comfort and

- wind safety in urban areas: General decision framework and case study for the Eindhoven University campus. *Environ. Model. Softw.* **30**, 15–34 (2012).
33. Tominaga, Y., Mochida, A., Yoshie, R., Kataoka, H., Nozu, T., Yoshikawa, M. & Shirasawa, T. AIJ guidelines for practical applications of CFD to pedestrian wind environment around buildings. *J. Wind Eng. Ind. Aerodyn.* **96**, 1749–1761 (2008).
 34. Franke, J., Hirsch, C., Jensen, A. G., Krus, H. W., Schatzmann, M., Miles, P. S. W. and S. D., Wisse, J. A. & Wright, N. G. Recommendations on the Use of CFD in Wind Engineering. *Cost Action C* 1–11 (2004).
 35. Franke, J. & Baklanov, A. *Best practice guideline for the CFD simulation of flows in the urban environment: COST action 732 quality assurance and improvement of microscale meteorological models.* (2007).
 36. Hirsch, C., Bouffieux, V. & Wilquem, F. CFD simulation of the impact of new buildings on wind comfort in an urban area. *Work. Proceedings, cost action C* **14**, 3–4 (2002).
 37. Bakker, A. Lecture 6 - Boundary Conditions Applied Computational Fluid Dynamics. *Fluid Dyn.* 1–31 (2006).
 38. Launder, B. E. & Spalding, D. B. The numerical computation of turbulent flows. *Comput. Methods Appl. Mech. Eng.* **3**, 269–289 (1974).
 39. Li, X. X., Liu, C. H., Leung, D. Y. C. & Lam, K. M. Recent progress in CFD modelling of wind field and pollutant transport in street canyons. *Atmos. Environ.* **40**, 5640–5658 (2006).
 40. ANSYS. 15. Discrete Phase. (2009). Available at:
<http://www.afs.enea.it/project/neptunius/docs/fluent/html/th/node238.htm>.
 41. ANSYS. 23.1.2 Limitations. (2009). Available at:
<http://www.afs.enea.it/project/neptunius/docs/fluent/html/ug/node669.htm#sec-disp-oview-limits>.

42. Rodes, C., Smith, T., Crouse, R. & Ramachandran, G. Measurements of the size distribution of aerosols produced by ultrasonic humidification. *Aerosol Sci. Technol.* **13**, 220–229 (1990).
43. Santiago, J. L., Martilli, A. & Martín, F. CFD simulation of airflow over a regular array of cubes. Part I: Three-dimensional simulation of the flow and validation with wind-tunnel measurements. *Boundary-Layer Meteorol.* **122**, 609–634 (2007).
44. Blocken, B., Carmeliet, J. & Stathopoulos, T. CFD evaluation of wind speed conditions in passages between parallel buildings-effect of wall-function roughness modifications for the atmospheric boundary layer flow. *J. Wind Eng. Ind. Aerodyn.* **95**, 941–962 (2007).
45. ANSYS. 7.6.1 Profile specification types. (2009). Available at:
<http://www.afs.enea.it/project/neptunius/docs/fluent/html/ug/node264.htm>.
46. Ranz, W. E. & Marshall, W. R. Evaporation from drops. *Chemical Engineering Progress* **48**, 141–148 (1952).
47. DePaul, F. T. & Sheih, C. M. Measurements of wind velocities in a street canyon. *Atmos. Environ.* **20**, 455–459 (1986).
48. Highsmith, V. R., Rodes, C. E. & Hardy, R. J. Indoor particle concentrations associated with use of tap water in portable humidifiers. *Environ. Sci. Technol.* **22**, 1109–1112 (1988).